THE JOURNAL OF PHYSICAL CHEMISTRY A
A JOURNAL OF THE AMERICAN CHEMICAL SOCIETY

pubs.acs.org/JPCA

Article

Electronic Spectroscopy of *cis*- and *trans-meta*-Vinylbenzyl Radicals

Sederra D. Ross, Jonathan Flores, Daniel M. Hewett, and Neil J. Reilly*

Cite This: *J. Phys. Chem. A* 2021, 125, 6420–6436

Read Online

ACCESS | Metrics & More | Article Recommendations | Supporting Information

ABSTRACT: The $D_0(^2A'')-D_1(^2A'')$ electronic transition of resonance-stabilized radical C_9H_9 isomers *cis*- and *trans-meta*-vinylbenzyl (MVB) has been investigated using resonant two-color two-photon ionization (R2C2PI) and laser-induced fluorescence. The radicals were produced in a discharge of *m*-vinyltoluene diluted in Ar and probed under jet-cooled conditions. The origin bands of the *cis* and *trans* conformers are at 19 037 and 18 939 cm^{-1}, respectively. Adiabatic ionization energies near 7.17 eV were determined for both conformers from two-color ion-yield scans. Dispersed fluorescence (DF) was used to conclusively identify the *cis*-conformer: ground-state *cis*-MVB eigenvalues calculated for a Fourier series fit of a computed vinyl torsion potential are in excellent agreement with torsional transitions in the 19 037 cm^{-1} DF spectrum. R2C2PI features arising from *cis*- or *trans*-MVB were distinguished by optical–optical hole-burning spectroscopy and vibronic assignments were made with guidance from density functional theory (DFT) and time-dependent density functional theory (TDDFT) calculations. There is a notable absence of mirror symmetry between excitation and emission spectra for several totally symmetric modes, whereby modes that are conspicuous in emission are nearly absent in excitation, and *vice versa*. This effect is largely ascribed to interference between Franck–Condon and Herzberg–Teller contributions to the electronic transition moment, and its pervasiveness a consequence of the low symmetry (C_s) of the molecule, which permits intensity borrowing from several relatively bright electronic states of A'' symmetry.

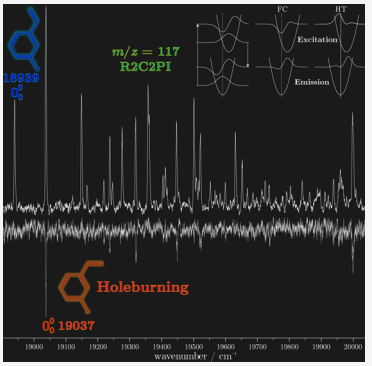

1. INTRODUCTION

Resonance-stabilized radicals (RSRs) are profoundly important intermediates in combustion and pyrolysis. They are formed preferentially during thermal decomposition of hydrocarbons[1,2] and are slow to further decompose or react with oxygen,[3] allowing their accumulation in flames. Recombination reactions involving propargyl (C_3H_3),[4−6] cyclopentadienyl (C_5H_5),[7,8] and benzyl (C_7H_7)[9−11] are considered the major pathways to benzene and naphthalene under combustion conditions. Similar chemistry is invoked in stellar outflows to explain the formation of polycyclic aromatic hydrocarbons,[12,13] the presumed carriers of infrared emission observed in diverse astrophysical environments.[14] Recent ground-breaking work by Johansson et al. has shown that extension of radical delocalization through covalent clustering reactions of RSRs is a key driver of the transition from molecular to particulate material during soot formation.[15]

To unravel molecular growth and decomposition pathways in energetic environments, diagnostic gas-phase spectroscopic data on putative reactive intermediates is essential. The D_0-D_1 electronic transitions of RSR chromophores generally appear in the optical band and often submit to interrogation by fluorescence and mass-resolved spectroscopies. In the past ∼15 years in particular, a slew of previously unknown RSRs of interest to combustion and astrochemistry have been characterized by these means, as reviewed recently.[16] Still, many more important radicals await spectroscopic observation. For a given molecular formula, a daunting variety of isomers are energetically accessible under combustion conditions. The C_7H_7 surface, for example, harbors at least 10 resonance-stabilized minima within 300 kJ/mol of the global minimum.[17,18] With increasing molecular mass, isomer-specific product identification by photoionization mass spectrometry, as in ref 15, can become intractable, highlighting a need for complementary optical assays.

To this end, we have set out to optically detect new RSRs under jet-cooled conditions by laser-induced fluorescence (LIF) and resonant two-color two-photon ionization (R2C2PI). Recently, in discharges of various precursors including toluene, we identified 3-ethynylcyclopentenyl, a C_7H_7 RSR bearing the 1-vinylpropargyl chromophore.[23] Here, we focus on the less-explored C_9H_9 surface. Figure 1 shows the low-lying phenyl-containing C_9H_9 RSRs discussed in this work, with relative energies compiled from refs 19–22. The 1-indanyl radical was the first isomer to be observed under jet-cooled conditions,[19] followed shortly afterward by *trans*-1-phenylallyl.[20,21] The former system is π-isoelectronic with benzyl, reflected in the small red shift of its D_0-D_1 origin (near 472.6 nm) relative to benzyl (near 454.4 nm). The 1-

Received: May 21, 2021
Revised: June 24, 2021
Published: July 14, 2021

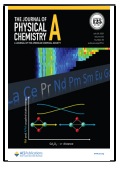

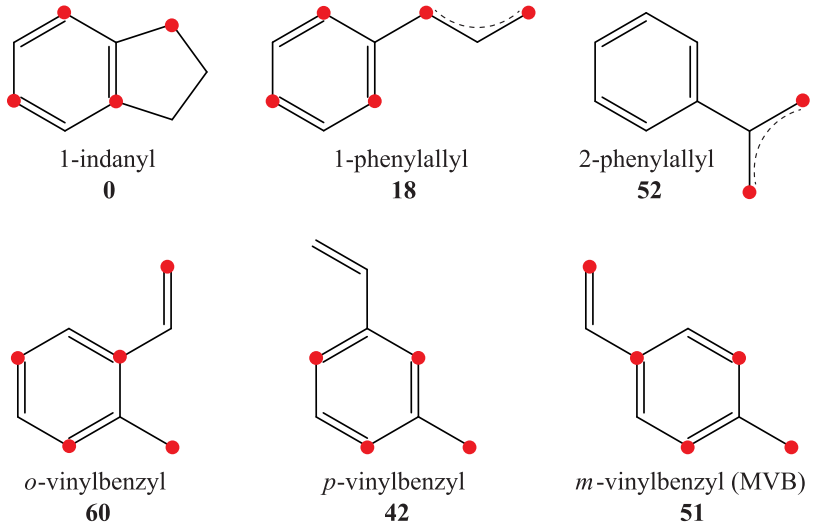

Figure 1. Low-lying resonance-stabilized radical isomers of C_9H_9. A red circle indicates the radical site in one of the multiple resonance structures that can be drawn for each isomer. Energies are reported in kJ/mol relative to 1-indanyl, the global minimum.[19−22] Only 1-indanyl and 1-phenylallyl have been observed spectroscopically.[20,21]

phenylallyl and benzyl radicals have the same highest occupied molecular orbital−lowest unoccupied molecular orbital (HOMO−LUMO) gap at the Hückel level (β), but depression of the lowest excited state of 1-phenylallyl by configuration interaction shifts its D_0−D_1 origin substantially, to 521 nm. The 2-phenylallyl radical probably absorbs modestly to the red of allyl (408 nm), but it has a lower resonance-stabilization energy,[20] and remains undiscovered.

No other C_9H_9 RSR has been conclusively identified, but other C_9H_9 band systems have been reported. In a discharge of 1,6-heptadiyne (C_7H_8), Steglich et al. observed an unknown number of C_9H_9 isomers in the region 630−550 nm by R2C2PI.[22] Intriguingly, several features were observed near diffuse interstellar band wavelengths (though near coincidences are not unlikely owing to the high spectral density of the DIBs). Because of their low ionization potentials (generally <8 eV), it would seem unlikely that neutral RSRs can survive in diffuse clouds (wherein 98% of C_{60}, with an IP near 7.6 eV, is ionized[24]); nevertheless, the authors suggested that neutral species derived from recombination of electrons with small cations may be of relevance to the DIB conundrum. An IP of 7.3 ± 0.1 eV was recorded for the carrier of an origin band near 629 nm. From this information and TD-B3LYP calculations, *o*-, *p*-, and *m*-vinylbenzyl radicals were suggested as the most plausible carriers.

The vinylbenzyl systems should be generously resonance-stabilized and readily produced by cleavage of the weakest C−H bond in the parent vinyltoluenes. Herein, we describe the first observation, and a quite comprehensive isomer-specific assignment, of the *cis*- and *trans*-vinylbenzyl D_0−D_1 transition. A Franck−Condon description of band intensities is rendered largely inutile by pronounced Herzberg−Teller activity in most totally symmetric vibrations. It emerges that probably no vinylbenzyl radical carries the 630−500 nm bands; promising candidates bearing cyclopentenyl groups are briefly discussed.

2. EXPERIMENTAL SECTION

MVB was produced using a pulsed discharge nozzle,[25] comprising a series of annular electrodes and Teflon insulators affixed to a pulsed valve with a 0.5 mm orifice. The precursor, *meta*-vinyltoluene, was stored behind the nozzle and heated to 60 °C, and the vapor entrained in Ar at 3 atm. A high-voltage pulse (typically 600−1000 V, 50 μs, 50 kΩ ballast resistance) was applied across the electrodes in synchronization with the leading edge of the gas pulse. The products were cooled to ∼15 K by supersonic expansion into vacuum.

Two vacuum chambers were used for this work: one for R2C2PI and one for LIF/DF (dispersed fluorescence). In R2C2PI, jet-cooled MVB radicals were admitted through a 2 mm skimmer into the extraction region of a time-of-flight mass spectrometer. There, they were exposed to tunable radiation (535−480 nm, 10 mJ/pulse) from a Nd:YAG-pumped pulsed dye laser, followed ∼10 ns afterward by UV radiation from a frequency-quadrupled Nd:YAG beam (266 nm, 0.5 mJ/pulse) or a KrF excimer (248 nm, 5 mJ/pulse). The nascent ions were extracted into a 1 m field-free drift tube and detected with a tandem microchannel plate. For adiabatic ionization energy (AIE) measurements, one dye laser was tuned to the origin transition of one or other MVB conformer, while the UV frequency-doubled output (250−270 nm, 0.5 mJ/pulse) of a second dye laser was scanned through the ionization threshold. Ion signal at m/z = 117 was averaged over 64 shots and integrated as a function of the scanned wavelength, yielding an optical excitation spectrum or a resonant two-color ion-yield curve. The laser wavelength was calibrated with a wavemeter of absolute accuracy 0.2 cm^{-1}.

Mass-resolved optical−optical hole-burning scans were recorded in a four-beam experiment. The fundamental and frequency-doubled beams from one dye laser (the burn) were simultaneously copropagated to excite and ionize one conformer *via* its origin transition, the notion being that immediate removal of excited-state population by ionization might mitigate saturation. Approximately 500 ns afterward, the visible probe beam and a subsequent ionizing pulse (248 m or 266 nm) entered the chamber, both beams counter-propagated to the burn using a dichroic mirror. The probe was operated at 10 Hz and the burn at 5 Hz. By toggling the output polarity of a boxcar integrator gated over probe signal at m/z = 117, the 5 Hz signal was actively subtracted from the 10 Hz signal, yielding a difference in the probe spectrum when probe and

https://doi.org/10.1021/acs.jpca.1c04496
J. Phys. Chem. A 2021, 125, 6420−6436

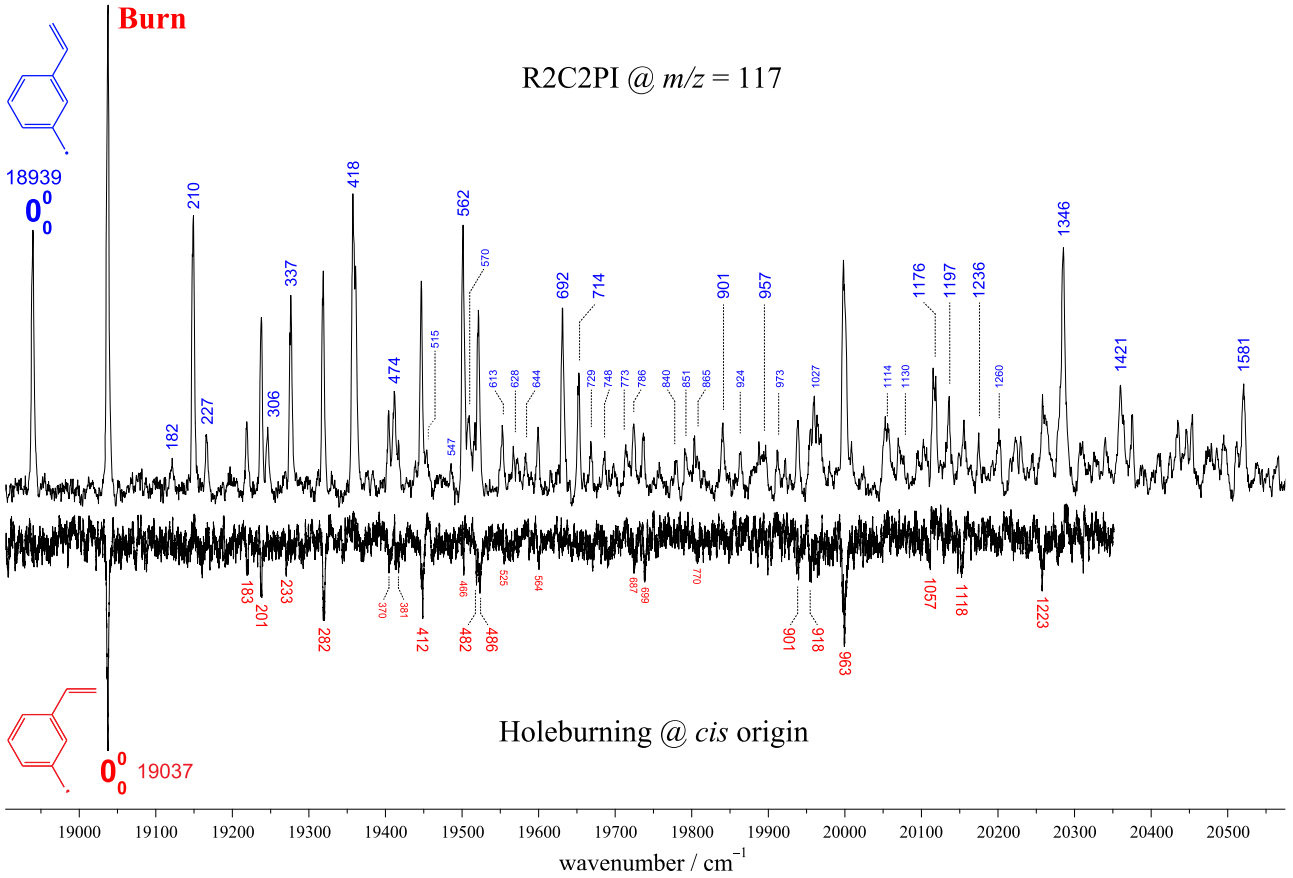

Figure 2. Upper trace: mass-selected R2C2PI spectrum of jet-cooled *m*-vinylbenzyl radical, produced in a jet-cooled *m*-vinyltoluene discharge. Reflected: optical−optical hole-burning spectrum recorded with the burn laser fixed to the origin transition of the *cis*-conformer. Vibronic band positions are reported relative to the *trans* and *cis* origin transitions, located at 18 939 and 19 037 cm^{-1}, respectively. Band assignments are given in Tables 1 and 2 and discussed in detail in Section 5.

burn interrogated transitions originating from the vibrationless level of the same conformer.

The LIF chamber is adapted from one first described in ref 26. Jet-cooled MVB radicals were exposed to tunable dye laser output approximately 25 mm downstream of the discharge aperture. Laser-induced emission was detected with a photomultiplier tube after being imaged through a small (0.14 m focal length) or a large (1 m focal length) monochromator. The small monochromator serves as a broad-bandpass filter in excitation scans; the large monochromator is equipped with a 1200 lines/mm grating and is used for DF spectroscopy. The latter instrument was operated with 0.6 mm slits, corresponding to a bandpass of ∼20 cm^{-1}. In DF scans, typically 64 fluorescence decay profiles were averaged and integrated over three temporal gates: one for scattered laser light, and the others for prompt (100 ns) and for slower (2 μs) decay, to identify possible contaminant features from species with significantly different fluorescence lifetimes.

3. COMPUTATIONAL DETAILS

Optimized geometries and harmonic vibrational frequencies of the neutral ground (D_0) and first excited (D_1) states of *cis*- and *trans*-MVB, as well as their cation singlet ground states, were obtained from density functional theory (DFT) and time-dependent density functional theory (TDDFT) calculations using the B3LYP functional with 6-311G++(d,p) basis set. The results were used to predict AIEs and D_0−D_1 transition energies, simulate rotational contours, and calculate Duschinsky matrices and band intensities in the Franck−Condon (FC) and Franck−Condon−Herzberg−Teller (FCHT) approximations. The FC factors and HT (*i.e.*, linear) transition moments were computed by the procedure of Barone et al.[27] as implemented in *Gaussian 09*.[28] The effects of Duschinsky rotation are included. AIEs were also predicted from CBS-QB3 calculations for the D_0 and S_0 states of the neutral and the cation, respectively, to help confirm the identification of MVB. It has been shown that the B3LYP/6-311G++(d,p)[20] (respectively, CBS-QB3[23]) AIEs of hydrocarbon RSRs are, on average, ∼0.1 eV lower (respectively, higher) than observation, on which basis our calculations should bracket experiment.

Ground- and excited-state vinyl torsion (ν_{48}) potentials were obtained from relaxed B3LYP/TD-B3LYP scans of the vinyl−phenyl dihedral angle. The calculation of torsional eigenvalues and eigenfunctions from Fourier series fits to the B3LYP potentials is described in Section 4.2 and the Supporting Information, Section S2. In Franck−Condon simulations, the B3LYP D_0 frequencies of 47 small-amplitude modes were scaled by 0.97, in accordance with usual practice for hydrocarbon RSRs.[20,29,30] While various scaling factors in the range 0.95−0.97 have previously been used[20,21,31,32] for excited states, we have left all D_1 frequencies unscaled. All calculations were performed with the *Gaussian 09* suite of electronic structure programs.[28]

https://doi.org/10.1021/acs.jpca.1c04496
J. Phys. Chem. A 2021, 125, 6420−6436

4. RESULTS

4.1. Identification of *m*-Vinylbenzyl Radical. The top trace of Figure 2 is the m/z = 117 R2C2PI spectrum of the *m*-vinyltoluene discharge in the region 18 900−20 600 cm^{-1} (*ca.* 530−485 nm); reflected is the m/z = 117 hole-burning spectrum recorded with the burn laser at 19 037 cm^{-1}. Part of the spectrum was also measured with the burn at 18 939 cm^{-1} (see the Supporting Information, Figure S1), but the weaker *trans* transition makes for relatively inefficient population depletion. The assignments for *cis*- and *trans*-MVB are given in Tables 1 and 2, respectively; they are discussed in detail in Section 5. Because substituted benzyl radicals can undergo facile configurational isomerization in discharges,[33] we first prove the chemical identities and conformations of the carriers. There is little doubt that every feature in the spectrum arises from a conformer of MVB. One, indanyl absorbs much further to the blue, with an origin near 21 159 cm^{-1},[19] and we find no evidence near 19 208 cm^{-1} of the phenylallyl D_0−D_1 origin, which dominates the phenylallyl spectrum.[20,21] Second, the features in Figure 2 are absent or greatly diminished when other C_9H_{10} precursors are used.

Third, the AIEs of the carriers of the bands at 19 037 and 18 939 cm^{-1} (7.168 and 7.165 eV, respectively, with uncertainties of 2.5 meV) are both close to 7.17 eV (Figure 3). The two-color ion-yield scans were recorded with an electric field of 200 V/cm in the extraction region of the ToF spectrometer; the field-free AIEs are at most 0.01 eV higher[34] than the indicated thresholds. They are thus consistent with MVB AIEs from B3LYP/6-311++G(d,p) (7.12 eV) and CBS-QB3 (7.22 eV) calculations (Table 3), which tend to bracket experiment by *ca.* 0.1 eV,[20,23] while calculated AIEs of *o*- and *p*-vinylbenzyl are below 7.1 eV, and that of 2-phenylallyl is above 7.7 eV.[22]

Finally, MVB is the only isomer in Figure 1 for which the calculated AIE and D_0−D_1 transition energy are both close to the experiment (Table 3). For both conformers, T_e is 2.48 eV; inclusion of ZPE gives T_0 = 2.42 eV for *cis* (*cf.* 2.36 eV observed), and T_0 = 2.35 eV for *trans* (*cf.* 2.35 eV observed). In fact, an excellent estimate for T_0 can be obtained without resorting to theory. As suggested in Figure 1, and in contrast to *ortho*- and *para*-MVB, the vinyl group does not participate in radical delocalization, in the sense that no reasonable Lewis structure can be drawn with a vinyl carbon hosting an unpaired

Table 1. Assignments for the R2C2PI Spectrum of *cis*-*m*-Vinylbenzyl Radical[a]

$\Delta\nu$ (cm^{-1})	assignment	$\Delta\nu$	assignment
0	0_0^0	564	$46_0^2 48_0^2$
183	48_0^2	687	$31_0^1 33_0^1$
201	33_0^1	699	$32_0^1 46_0^1 48_0^1$
233	$47_0^1 48_0^1$	770	$31_0^1 46_0^1 48_0^1$
282	$46_0^1 48_0^1$	901	27_0^1
370	48_0^4	918	26_0^1
381	$33_0^1 48_0^2/46_0^2$	963	25_0^1
412	$32_0^1/33_0^2$	1057	22_0^1
466	$46_0^1 48_0^3$	1118	21_0^1
482	$33_0^1 46_0^1 48_0^1$	1223	16_0^1
486	31_0^1	1244	$25_0^1 46_0^1 48_0^1$
525	29_0^1		

[a]Band positions are reported relative to the origin at 19 037 cm^{-1}.

Table 2. Assignments for the R2C2PI Spectrum of *trans*-*m*-Vinylbenzyl Radical[a]

$\Delta\nu$ (cm^{-1})	assignment	$\Delta\nu$	assignment
0	0_0^0	748	$29_0^1 48_0^2$
182	48_0^2	758	$10_0^1 30_0^1$
210	33_0^1	773	$29_0^1 33_0^1$
227	$46_0^1 48_0^1$	786	$29_0^1 46_0^1 48_0^1$
306	32_0^1	840	30_0^2
337	10_0^1	851	$30_0^1 33_0^2$
382	$33_0^1 48_0^2$	865	$29_0^1 32_0^1$
418	$30_0^1/33_0^2$	901	$27_0^1/\ 10_0^1 29_0^1$
437	$33_0^1 46_0^1 48_0^1$	924	$28_0^1 46_0^1 48_0^1$
445	$46_0^2 48_0^2$	957	26_0^1
474	31_0^1	973	$29_0^1 30_0^1$
515	$32_0^1 33_0^1$	1027	$10_0^1 28_0^1$
547	$10_0^1 33_0^1$	1114	$28_0^1 30_0^1$
562	29_0^1	1130	29_0^2
570	$10_0^1 46_0^1 48_0^1$	1176	22_0^1
613	32_0^2	1197	21_0^1
628	$30_0^1 33_0^1$	1236	19_0^1
644	$10_0^1 32_0^1$	1260	$28_0^1 29_0^1$
675	10_0^2	1285	$29_0^1 30_0^1 32_0^1$
692	28_0^1	1346	$18_0^1/\ 16_0^1$
714	$30_0^1 32_0^1$	1421	11_0^1
729	$32_0^1 33_0^2$	1581	20_0^1

[a]Band positions are reported relative to the origin at 18 939 cm^{-1}.

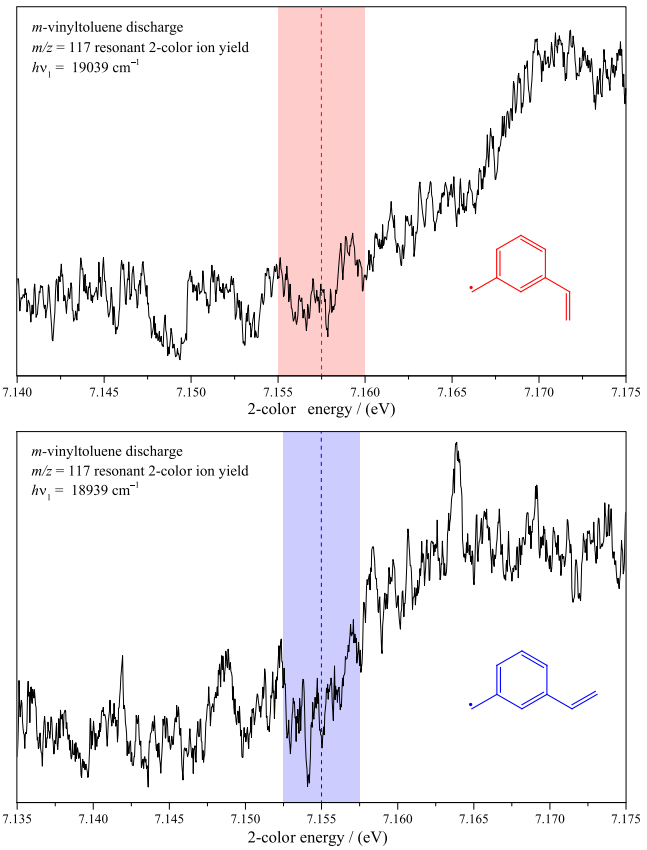

Figure 3. Mass-selected two-color ion-yield scans of *cis*- and *trans*-*m*-vinylbenzyl radical, measured *via* their respective origin transitions. The shaded regions represent confidence intervals of 2.5 meV for experimental thresholds. The field-free AIEs are at most 0.01 eV higher than the vertical dashed lines.

https://doi.org/10.1021/acs.jpca.1c04496
J. Phys. Chem. A 2021, 125, 6420−6436

Table 3. Calculated and Observed Ionization (AIE) and D_0−D_1 Transition Energies of MVB[a,b]

property	*cis*-MVB	*trans*-MVB
relative energy (cm^{-1})	134*/127	0
calculated AIE w. ZPE (eV)	7.22*/7.12	7.22*/7.12
observed AIE (eV)	7.168(3)	7.165(3)
calculated T_e (eV)	2.48	2.48
calculated T_0 (eV)	2.42	2.36
observed T_0 (eV)	2.36	2.35

[a]Asterisked quantities are from CBS-QB3 calculations; all other calculated properties derive from B3LYP/6-311G++(d,p) geometries and frequencies. [b]The observed AIEs include a +0.01 eV empirical correction to account for the static electric field (240 V/cm) in the ToF mass spectrometer.

electron. From this viewpoint, MVB can be described as containing a vinyl-substituted benzyl chromophore, and it is illuminating to compare the benzene/benzyl system to its vinyl-substituted equivalent, styrene/*m*-vinylbenzyl. The benzyl D_0−D_1 origin is at 22 002 cm^{-1} and the S_0−S_1 band-gap of benzene, neglecting the ∼600 cm^{-1} inducing mode ν_6, is *ca.* 38 000 cm^{-1}, giving an electronic red shift from benzene to benzyl of approximately 16 000 cm^{-1}. Application of this red shift to the styrene S_0−S_1 transition, with origin at 34 760 cm^{-1}, yields a prediction of *ca.* 18 800 cm^{-1} for the MVB D_0−D_1 origin, in remarkable accord with the observed *trans*-MVB origin at 18 939 cm^{-1}(Tables 4).

Table 4. Assignments for the Origin Dispersed Fluorescence Spectrum (Figure 6) of *cis-m*-Vinylbenzyl Radical[a]

$\Delta\nu$ (cm^{-1})	assignment	$\Delta\nu$ (cm^{-1})	assignment
0	0_0^0	987	25_1^0
73	48_2^0	1061	$25_1^0 48_2^0$
170	48_4^0	1168	$21_1^0/22_1^0$
369	32_1^0	1250	20_1^0
444	31_1^0	1310	$17_1^0/18_1^0/20_1^0 48_2^0$
535	$30_1^0/29_1^0$	1374	$17_1^0 48_2^0/18_1^0 48_2^0$
609	$30_1^0 48_2^0$	1569	11_1^0
732	28_1^0	1643	$10_1^0/11_1^0 48_2^0$
804	$28_1^0 48_2^0$	1715	$10_1^0 48_2^0$
917	27_1^0		

[a]Band positions are reported as Stokes shift from the pump frequency (19 037 cm^{-1}).

While it is thus clear that MVB is responsible for the m/z = 117 R2C2PI spectrum, it is far from obvious which conformer carries which band system. The carrier AIEs differ by at most a few meV, which margin cannot be captured by any practicable calculation. The cation S_0 state is predicted to be planar for *trans*; for *cis*, the calculated vinyl−phenyl dihedral angle in S_0 is *ca.* 158°. One might therefore expect a relatively gradual onset in the *cis*-2-color ion-yield curve due to off-diagonal Franck−Condon activity in the vinyl torsion, an interpretation that appears to be at least qualitatively correct (see FC simulations, based on $S_0 \leftarrow D_1$ FC factors calculated using FCLab II,[35,36] in the Supporting Information, Section S4). The TD-B3LYP results imply *cis*-MVB absorbs to the blue of *trans*-MVB, consistent with our analysis, but again the difference is marginal, and the similar closed-shell systems *m*-fluorostyrene,[37,38] *m*-chlorostyrene,[39] and *m*-methylstyrene[40] show the opposite trend. Simulated origin band envelopes using calculated rotational constants and transition moments (Figure 4) are not inconsistent with our assignment—but nor, at our resolution, are they conclusive.

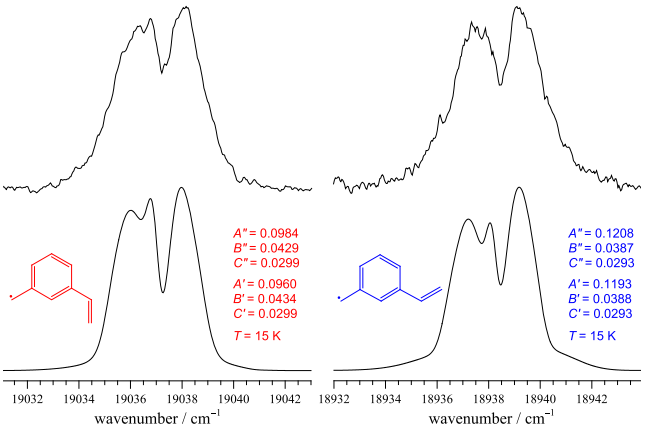

Figure 4. Profiles of the 19 037 and 18 939 cm^{-1} bands recorded by R2C2PI, and beneath, simulated rotational envelopes carried out with PGOPHER[41] using rotational constants and electronic transition moments from B3LYP/6-311++G(d,p) calculations. The ratio a/b of the *a*- and *b*-axis-polarized transition moments is 1.9:1 for *cis*-MVB and 1.2:1 for *trans*-MVB.

Moreover, B3LYP *cis* and *trans* D_1 frequencies (Table 5; see Section 5) do not, unsurprisingly, differ considerably, and thus compare nearly equally well with both band systems. The D_0−D_1 transition also engenders comparable Franck−Condon activity in the two conformers (Section 5), but curiously, only the 19 037 cm^{-1} band system is origin-dominated. In short, it is difficult to make unambiguous isomer-specific assignments from R2C2PI alone. On the other hand, inspection of the calculated properties in Tables 3 and 5 reveals the D_0 vinyl torsion frequency to present a major point of difference. Indeed, relaxed scans (Figure 5) of the vinyl−phenyl dihedral angle suggest that while both D_1 wells and the D_0 *trans* well are roughly harmonic at low energies, the D_0 *cis* well is relatively flat-bottomed. To exploit the conformational specificity of the D_0 vinyl torsion, we turn to dispersed fluorescence spectroscopy.

4.2. Distinguishing the *cis*- and *trans*-MVB Band Systems. Figure 6 shows the DF spectrum of the 19 037 cm^{-1} band. Its full assignment and the simulations beneath are discussed in Section 5. For now, we focus on the strong band at 73 cm^{-1}. It can have no assignment other than 48_2^0, with ν_{48} being the vinyl torsion, which is of *a″* symmetry and governed by the selection rule $\Delta\nu = \pm 2$. How does this compare with theory? For *trans*-MVB, the B3LYP D_0 ν_{48} frequency is 51 cm^{-1} using the 6-311++G(d,p) and cc-PVTZ basis sets, yielding a harmonic prediction of 102 cm^{-1} for $2\nu_{48}$; for *cis*, we obtain 15 cm^{-1} (6-311++G(d,p)) and 35 cm^{-1} (cc-PVTZ), giving predictions of 30 and 70 cm^{-1}. Allowing for the negative anharmonicity expected for a flat-bottomed potential, the *cis* isomer is perhaps the better candidate; but to allay doubt, the eigenvalues of the torsional potentials in Figure 5 should be calculated.

The Schrödinger equation for internal rotation of a rigid top attached to a rigid frame is

https://doi.org/10.1021/acs.jpca.1c04496
J. Phys. Chem. A 2021, 125, 6420−6436

Table 5. Calculated (B3LYP/6-311++G(d,p)) Frequencies, Excluding the Nine a' CH-Stretch Modes, for the D_0 and D_1 States of MVB[a]

		cis-MVB		*trans*-MVB		
mode	symm.	D_0	D_1	D_0	D_1	description
10	a'	1684 *1643*	1661	1683	375 *338*	vinyl C=C stretch
11	a'	1594 *1569*	1562	1593	1508 *1421*	ϕ-deform./C2C3 + C4C5 stretch
12	a'	1577	1482	1570	1467	ϕ-deform./C1C4 + C3C6 stretch
13	a'	1499	1455	1503	1426	ϕ-CH wag + HC3′H bend
14	a'	1490	1524	1491	1489	HC3′H bend
15	a'	1461	1469	1462	1468	vinyl CH_2 bend/ϕ-deform.
16	a'	1434	1321 [*1221*]	1423	1394 [*1346*]	vinyl CH_2 bend/ϕ-deform.
17	a'	1348	1351	1348	1331	ϕ-CH wag
18	a'	1343 *1310*	1301	1344	1381 *1346*	Kekulé mode/CH wag
19	a'	1317	1378 [*1323*]	1315	1260 [*1236*]	Kekulé mode/CH wag
20	a'	1272 *1250*	1238	1293	1665 *1581*	C3C3′ stretch/ϕ-deform.
21	a'	1191 *1168*	1182 [*1115*]	1199	1211 [*1197*]	CH bend/ϕ-deform.
22	a'	1180	1136 [*1055*]	1182	1169 *1176*	CH bend/ϕ-deform.
23	a'	1113	1094	1125	1117	CH bend/ϕ-deform.
24	a'	1080	1057	1041	1021	CH bend/vinyl CH_2 rock
25	a'	998 *987*	991 *962*	1002	1012	ϕ-breathe/CH_2 rock
26	a'	987	942	986	993 *958*	CH_2 rock/ϕ-breathe
27	a'	925 *917*	892 [*901*]	928	898 [*901*]	ϕ-deform./CH_2rock
28	a'	739 *732*	721	741	728 *692*	ϕ-deform./C1C1′ stretch
29	a'	558	536 [*525*]	584	580 *562*	ϕ-deform./vinyl CH_2 rock
30	a'	541 *535*	331	529 *521*	437 *418*	ϕ-deform.
31	a'	456 *444*	486 *486*	455 *449*	526 [*473*]	C1C1′C2′ bend/CH_2 wag
32	a'	370 *369*	378 *410*	347 *345*	311 *306*	CH_2/vinyl wag
33	a'	200	201 *201*	212 *218*	170 *210*	vinyl wag
34	a''	1026	973	1025	920	vinyl CH wag/vinyl CH_2 twist
35	a''	974	947	974	954	ϕ-CH wag
36	a''	932	870	932	810	vinyl CH_2 wag
37	a''	895	812	900	849	ϕ-CH wag
38	a''	888	777	885	794	ϕ-CH wag
39	a''	805	729	799	746	ϕ-CH wag
40	a''	730	850	738	725	HC′3H bend
41	a''	707	648	710	627	ϕ-CH wag
42	a''	662	567	665	569	bend about C3C4 axis
43	a''	510	480	507	493	ϕ-twist (*cis*)/HC3′H twist (*trans*)
44	a''	495	579	500	453	HC3′H twist (*cis*)/ϕ-twist (*trans*)
45	a''	405	370	414	383	ϕ-pucker
46	a''	211	202 *193*[d]	202	166 *138*[d]	bend about C1 + ϕ-twist/pucker
47	a''	183	155 *144*[d]	197	216	bend about C1 + ϕ-twist/pucker
48	a''	15 *37*[b]	94 *92*[c]	51	99 *91*[c]	vinyl torsion

[a]All frequencies are unscaled. Mode descriptions are based on the D_0 normal coordinates. "ϕ" denotes the phenyl ring. D_0 mode numbers follow the Mulliken convention, and D_1 modes are numbered in terms of the D_0 basis, according to the diagonal elements of the Duschinsky matrices in Figure 9. Experimental frequencies determined in this work are in italics; square brackets enclose frequencies from tentative assignments. [b]$0.5 \times 48_2$; the anharmonic value (Figure 7) is *ca.* 33 cm^{-1}. [c]0.5×48^2; the anharmonic value is *ca.* 89 cm^{-1} (see the Supporting Information, Section S2 and Figure S2). [d]Assumes anharmonic values for ν_{48} (see note *b*), and no anharmonic cross-terms (see also the Supporting Information, Section S2).

$$\left[-B\frac{d^2}{d\phi^2} + V(\phi)\right]\Psi_k(\phi) = E_k\Psi_k(\phi)$$

For vinyl torsion in MVB, ϕ is the dihedral angle between the vinyl and phenyl groups and B is the reduced rotational constant[42] of the vinyl top. To compute vibrational intervals for comparison with DF spectra, the potential of interest $V(\phi)$ is the relaxed D_0 vinyl−phenyl dihedral scan in Figure 5, which was fit, as is customary,[43] to a Fourier series of the form

$$V(\phi) = \frac{1}{2}\sum_{n=1}^{6} V_n(1 - \cos n\phi)$$

Because the *cis* and *trans* wells are not equivalent, it is necessary to admit an angular dependence of B. The D_0 and D_1 geometries obtained at each point of the relaxed scans (*i.e.*, 5° increments from 0 to 180°) were used to calculate the reduced moment of inertia and internal rotation constant of the vinyl top as a function of ϕ by the procedure of Wong.[44] The resulting function was fit to a six-term cosine expansion

$$B(\phi) = \sum_{n=1}^{6} B_n \cos n\phi$$

Following Laane,[45] the Hamiltonian matrix for the hindered rotor problem was set up in terms of the free rotor (*i.e.*, $V(\phi)$ =

https://doi.org/10.1021/acs.jpca.1c04496
J. Phys. Chem. A 2021, 125, 6420−6436

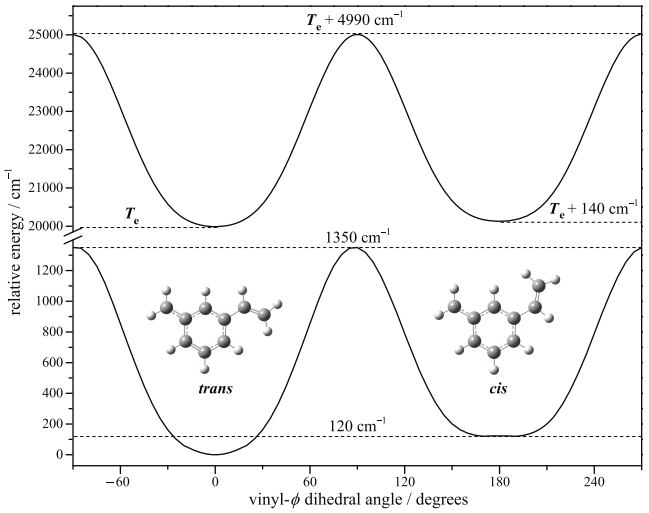

Figure 5. Relaxed scan of the vinyl−phenyl dihedral angle for *m*-vinylbenzyl radical (B3LYP/6-311++G(d,p)). T_e is the energy difference between the *trans* D_0 and D_1 minima (19 991 cm^{-1}), neglecting ZPE.

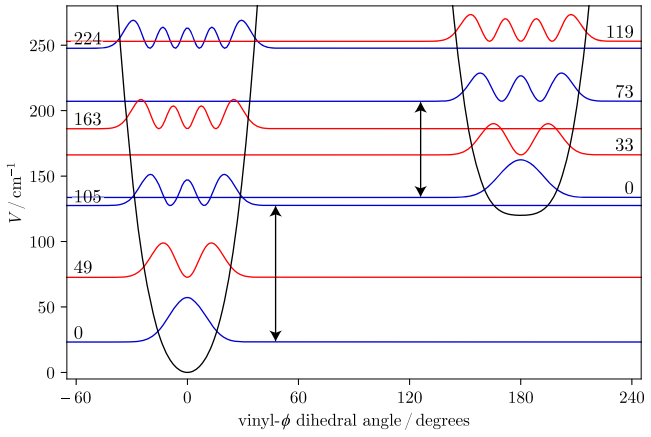

Figure 7. Eigenstate probability distributions and eigenvalues of the B3LYP ground-state vinyl torsion (ν_{48}) potential. The *trans* minimum is at 0°. Eigenstates of even and odd symmetry are indicated in blue and red, respectively. For each conformer, an arrow indicates the 0−2 torsional interval, corresponding to the lowest-frequency symmetry-allowed feature observable in emission from the D_1 vibrationless level (*cf.* 19 037 cm^{-1} DF spectrum in Figure 6).

0) basis functions $\Phi_m(\phi) = (2\pi)^{-1/2}e^{im\phi}$, which have eigenvalues $E_m = m^2B$, $m = 0, \pm1, \pm2$, *etc.* The symmetry properties of trigonometric functions admit a decomposition of the Hamiltonian matrix into an even (cosine) block and an odd (sine) block. The matrix was diagonalized to give the eigenvalues E_k and eigenfunctions $\Psi_k = \sum_m c_{mk}\Phi_m$. Fifty basis functions were more than sufficient to achieve satisfactory convergence of the eigenvalues.

Figure 7 shows the main results for the ground state (see also Figure S2 and Table S1); torsional intensities and D_1 eigenvalues are discussed in the Supporting Information, Section S2. The 73 cm^{-1} feature in the 19 037 cm^{-1} DF spectrum should be compared to the calculated ν_{48} 0−2 interval: 73 cm^{-1} for *cis*-MVB and 105 cm^{-1} for *trans*-MVB. The agreement is vastly superior for the *cis*-conformer, and further, the weak DF feature at 170 cm^{-1} accords with the calculated *cis*-MVB 0−4 interval (169 cm^{-1}). The low signal-to-noise ratio of the DF spectrum for the weaker origin at 18 939 cm^{-1} (Supporting Information, Figure S3) prevents us from identifying *trans* torsional transitions with confidence. Nevertheless, it exhibits no distinct reproducible features below 200 cm^{-1}, and the few bands observed are consistent

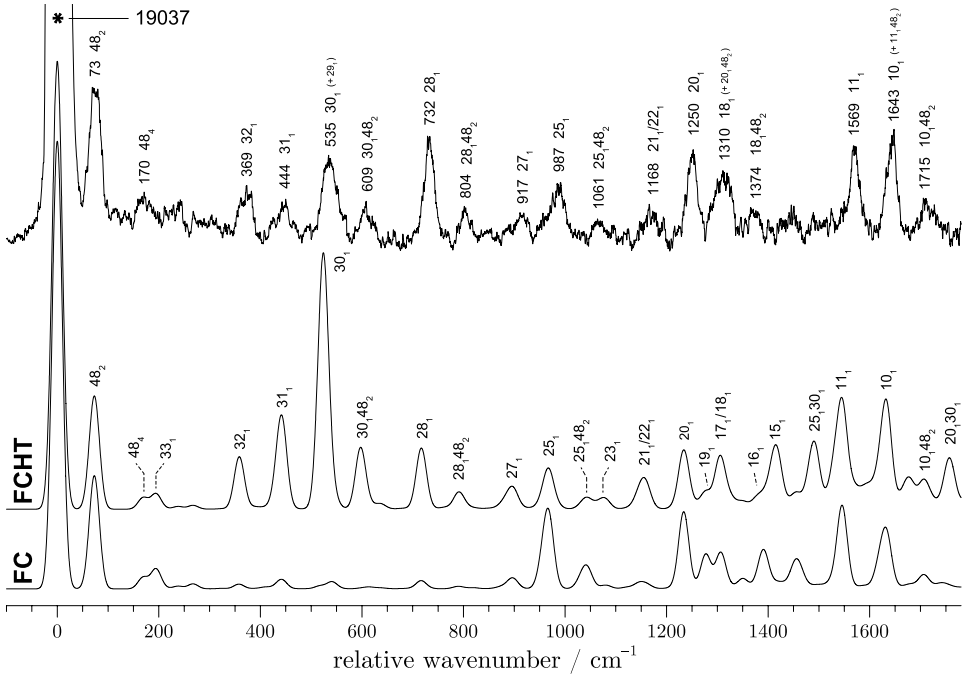

Figure 6. From top: Dispersed fluorescence spectrum observed by pumping the origin transition of *cis*-*m*-vinylbenzyl radical at 19 037 cm^{-1}, and simulations carried out within the Franck−Condon−Herzberg−Teller (FCHT) and Franck−Condon (FC) approximations. The calculation of vinyl torsional levels (ν_{48}) is described in Section 4.2. All other vibrational frequencies are from B3LYP/6-311++(d,p) calculations and have been scaled by 0.97. The assignments are given in Table 4 and discussed in Section 5.

https://doi.org/10.1021/acs.jpca.1c04496
J. Phys. Chem. A 2021, 125, 6420−6436

with *trans* D_0 frequencies, notably ν_{32} near 345 cm^{-1}. We therefore consider that the *cis* and *trans* band systems have been distinguished beyond doubt.

5. DETAILED ASSIGNMENTS AND DISCUSSION

5.1. Geometries, Frequencies, and Duschinsky Matrices. Figure 8 shows the optimized structures of the D_0 and D_1 states. The electronic transition is assigned as $A''-A''$, and as is typical for odd-alternant π-radical chromophores,[46,47] the D_1 state can be described as a superposition of nearly degenerate configurations derived from one-electron excitations into and out of the singly occupied orbital. The result of this configuration interaction is to diminish the D_0-D_1 transition moment, consistent with the small predicted *f*-values: 8×10^{-4} for *cis*-MVB and 3×10^{-4} for *trans*-MVB. For *cis*, the transition is mostly polarized along the *x*-axis (or *a*-axis), while for *trans*, the two in-plane components of μ are of similar size. The structural changes caused by electronic excitation involve lengthening of all C−C bonds by 0.01−0.04 Å, except for the C3′C3 and C1C1′ bonds, which are commensurately shortened. Both conformers are predicted to be planar in both states, and the only bond angle that changes significantly is ∠C1C1′C2, connecting vinyl and phenyl groups.

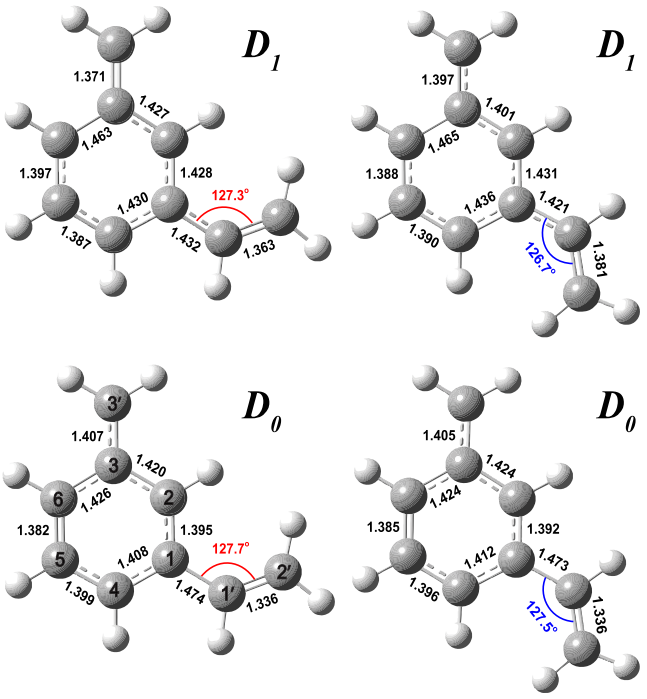

Figure 8. Optimized geometries of the ground (D_0) and first excited (D_1) states of *cis*- and *trans*-*m*-vinylbenzyl radical from B3LYP/TD-B3LYP calculations with 6-311G++(d,p) basis. Complete Cartesian coordinates are given in the Supporting Information.

On these premises, a' modes involving the carbon framework are expected to be Franck−Condon-active, particularly C−C stretch and ring-deforming modes, as well as the in-plane vinyl wag (ν_{33}). Neglecting anharmonic resonances, FC activity in a'' modes derives from changes in their force constants and is thus only expected to be noticeable for the vinyl torsion, ν_{48}, and modes with which it is Duschinsky-mixed (*vide infra*). The C1C1′ bond, connecting the vinyl group to the phenyl ring, shortens markedly (0.04−0.05 Å) upon excitation, causing the vinyl torsion frequencies and *cis*−*trans* isomerization barrier (Figure 5) to increase by a factor of several (though the true D_0 and D_1 barriers are probably smaller than theory indicates[48]).

Table 5 contains all unscaled D_0 and D_1 B3LYP/6-311G++(d,p) vibrational frequencies, neglecting the nine FC-inactive CH-stretch modes. We emphasize that while the D_0 mode labels follow the Mulliken convention, D_1 modes are numbered according to the Duschinsky matrices in Figure 9. To wit, for small displacements, the normal coordinates $\mathbf{Q}''$ and $\mathbf{Q}'$ of different electronic states can be related by the linear transformation[49]

$$\mathbf{Q}' = \mathbf{J}\mathbf{Q}'' + \mathbf{K}$$

where $\mathbf{K}$ is a $(3N-6)$-dimensional vector of displacements along the normal coordinates and $\mathbf{J}$ is the $(3N-6) \times (3N-6)$-dimensional Duschinsky (or rotation) matrix. Because MVB has C_s symmetry in both electronic states, the elements of $\mathbf{K}$ are necessarily zero for all a'' modes and $\mathbf{J}$ is block-diagonal with respect to symmetry species. Figure 9 shows the Duschinsky matrices for MVB, separated into a' and a'' blocks. For all but the *cis* a'' matrix, extensive mixing precludes a reordering of the columns such that the largest element is always on the diagonal. We have therefore arranged the columns to maximize the trace of each matrix and renumbered the D_1 modes in terms of the D_0 basis. The use of a single set of mode labels for both states in this manner greatly simplifies the discussion of spectral assignments.[29,31]

One important manifestation of Duschinsky mixing is the appearance of "forbidden" transitions involving nontotally symmetric modes (see, *e.g.*,[29,50,51]). If *X* and *Y* are mutually rotated a'' modes, the level X^1Y^1 contains the character of X^2 and Y^2 in terms of the ground-state basis, and the overlap integral for the otherwise forbidden transition $X_0^1Y_0^1$ can be significant. This is a well-known feature of electronic spectra of styrene[52,53] and substituted styrenes,[37,38,54,55] whereby electronic excitation mixes the vinyl torsion with low-frequency out-of-plane bending modes, allowing transitions of the type $X_0^nY_0^m$, where *n*, *m* are odd. The a'' matrices in Figure 9 imply that this effect should be in play for modes 46−48.

5.2. Franck−Condon Analysis. Franck−Condon simulations comprise the bottom traces ("FC") in Figure 6 (*cis*-MVB DF), Figure 11 (*cis*-MVB R2C2PI), and Figure 13 (*trans*-MVB R2C2PI). Herzberg−Teller effects will be discussed in the following section. Because B3LYP ground-state frequencies scaled by 0.97[56] agree reliably well with experiment,[20,29,30] it is simplest to assign the *cis*-MVB origin DF spectrum first (Figure 6). To begin, we note a recurring motif: every sufficiently strong feature—for example, at 535 cm^{-1} (presumably a blend, because of its width), 732, and 1643 cm^{-1}—has a weaker consort *ca.* 75 cm^{-1} to the blue. Further, the bands at 1310 and 1643 cm^{-1} are relatively broad, probably owing to overlap with +75 cm^{-1} satellites of strong bands at 1250 and 1569 cm^{-1}. Because the 48_2^0 band at 73 cm^{-1} dominates the spectrum, we interpret that the +75 cm^{-1} satellites are combinations of $2\nu_{48}$ with a' fundamentals. Calculated band intensities involving ν_{48} are not expected to be highly accurate because of anharmonicity and normal coordinate rotation (see further comments in Section 5.3 and the Supporting Information, Section S2). However, we note that the observed intensities of the satellites relative to the putative fundamentals are ∼0.2 to 0.3. To guide the eye, we have thus scaled combination bands of the form $X_1^048_2^0$ to have

https://doi.org/10.1021/acs.jpca.1c04496
J. Phys. Chem. A 2021, 125, 6420−6436

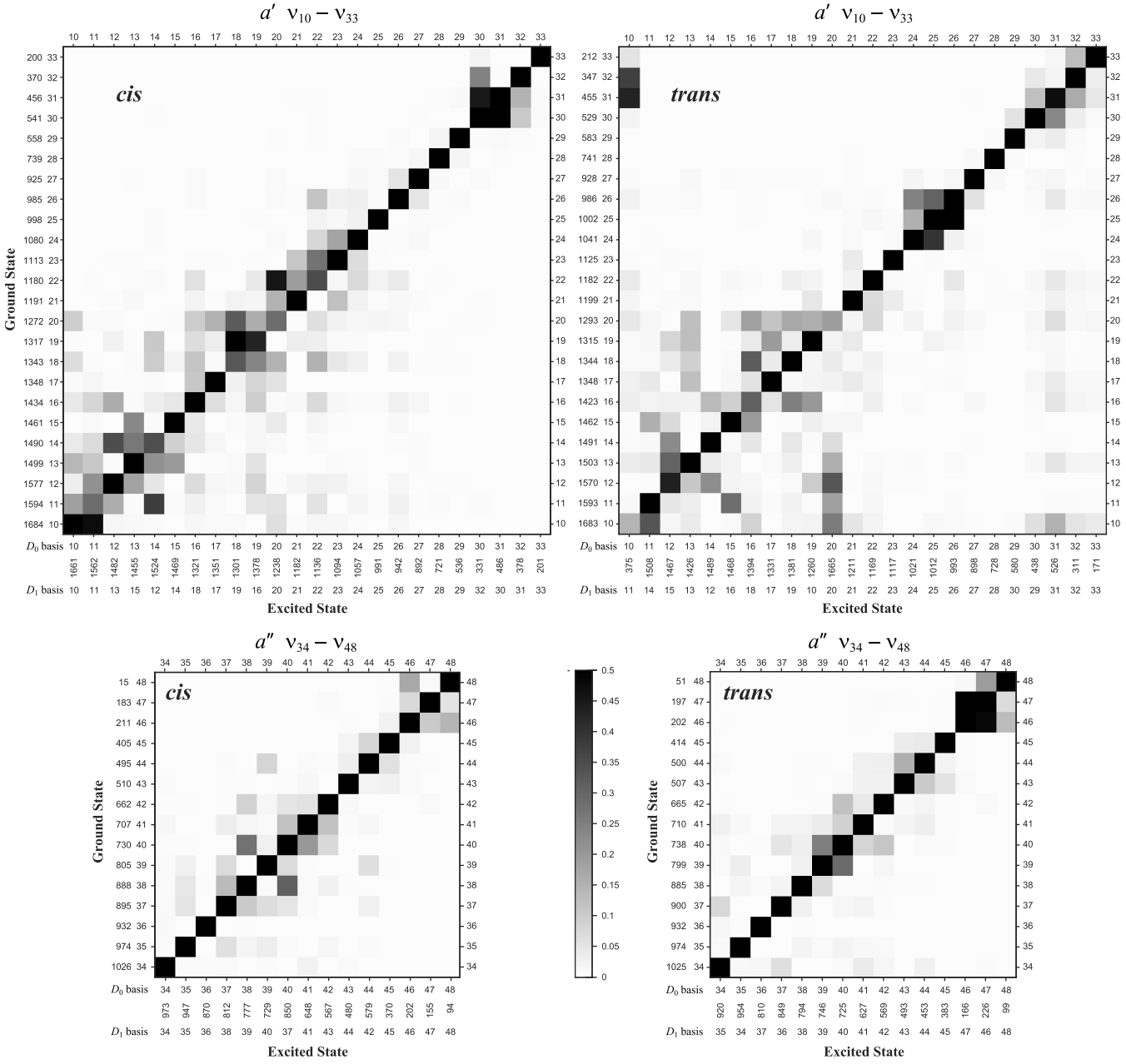

Figure 9. Duschinsky (rotation) matrices relating normal coordinates of the ground and first excited states of *cis*- and *trans-m*-vinylbenzyl radical. Ground-state mode labels strictly follow the Mulliken convention for C_s symmetry. The columns have been ordered such that the trace of each matrix is maximized, and D_1 modes are labeled throughout the text in terms of the D_0 basis.

25% of the intensity of the related X_1^0 false origins in the FC and FCHT simulations (this factor is similar to that observed for styrene, for which the vinyl torsion frequency is similarly affected by electronic excitation[57]). The assignment of the major features is subsequently quite straightforward—on the basis of calculated a' frequencies, at least. The observed and scaled B3LYP frequencies of the a' modes assigned in Figure 6 agree to within ∼1.5%, on average, and the mean absolute deviation is 13.0 cm^{-1} (see also the Supporting Information, Section S6).

Although experience with similar RSRs causes us to be confident in these assignments, the FC simulation is obviously grossly inaccurate throughout *ca.* 200−1000 cm^{-1}. The ν_{28}−ν_{32} fundamentals are expected to be weaker than 33_1^0, which is absent; the strongest observed a' fundamental, 28_1^0 at 732 cm^{-1}, has little FC intensity; and whereas the simulation implies a prominent 25_1^0 band (the ring-breathe) near 990 cm^{-1}, the observed feature is weak. The last point is surprising insofar as ring-breathe modes are often strongly FC-active in phenyl-containing chromophores. More curiously still the *cis*-MVB R2C2PI spectrum (Figure 11) is in several ways the reverse of the DF spectrum. For example, 25_0^1 is observed (at 963 cm^{-1}), but not predicted, to be the strongest band after the origin; similarly, 33_0^1 should be below the noise floor, but is detected readily at 201 cm^{-1}; and the most intense a' feature in emission, 28_1^0, has no counterpart in excitation.

Nor do the FC simulations capture significant qualitative differences between the *cis*-MVB and *trans*-MVB R2C2PI spectra (*cf.* Figures 11 and 13). For instance, while both conformers are predicted to have vastly origin-dominated

https://doi.org/10.1021/acs.jpca.1c04496
J. Phys. Chem. A 2021, 125, 6420−6436

transitions, several *trans* features rival or surpass the origin. Furthermore, for *trans*-MVB, the ring-breathe (ν_{26} in the *trans* excited state) has the strongest predicted FC activity, but is weak in the *trans*-MVB excitation spectrum—essentially the same trend observed for the analogous mode (ν_{25}) in emission for *cis*-MVB, but the opposite of its behavior in the *cis*-MVB excitation spectrum.

Most of the vibronic structure for both conformers unequivocally arises from a' fundamentals and not from vinyl torsion transitions (see the *trans*-MVB 0^0 + 210 cm^{-1} DF spectrum Figure S3 in the Supporting Information). The unusually comprehensive failure of the FC approximation, particularly below 1000 cm^{-1}, implies that the D_0−D_1 transition moment is strongly modulated by in-plane deformations of the carbon skeleton. The low symmetry of the molecule is of some import in this context. Distortion along a vibrational coordinate of symmetry Γ_{vib} can enhance the transition moment to an electronic state of symmetry Γ_{elec} if the product $\Gamma_{elec} \times \Gamma_{vib}$ contains the irrep of a bright state lying not too distant in energy. In relatively symmetric molecules, such as benzene (D_{6h}) and the *para*-dihalobenzenes (D_{2h}), this condition is not met readily. While vibronically induced transitions are of course well known in the S_0−S_1 spectra of these species (see, *e.g.*, refs 58 and 59), they manifest for only a small handful of modes, being in-plane deformations of symmetries e_{2g} in benzene and b_{3g} in the *para*-dihalobenzenes (and correlating with a' symmetry in a planar C_s molecule).

For the D_0−D_1 transition of MVB, the symmetry constraints for the vibronic acquisition of transition moment are much less onerous. Because the transition is dipole-allowed, a' modes can contribute additional oscillator strength. We calculate that four $^2A''$ excited states lie vertically within 2 eV of D_1 (Table 6);

Table 6. TD-BLYP/6-311G++(d,p) Electronic States, Vertical Transition Energies (eV), and Oscillator Strengths (f) of MVB

	state	ΔE	f
cis	$\tilde{X}\,^2A''$ (D_0)	0.00	
	$\tilde{A}\,^2A''$ (D_1)	2.62	0.0008
	$2\,^2A''$	3.01	0.0010
	$3\,^2A''$	3.19	0.0227
	$4\,^2A''$	3.46	0.0042
	$1\,^2A'$	4.32	0.0034
	$5\,^2A''$	4.47	0.0027
trans	$\tilde{X}\,^2A''$ (D_0)	0.00	
	$\tilde{A}\,^2A''$ (D_1)	2.62	0.0003
	$2\,^2A''$	3.12	0.0007
	$3\,^2A''$	3.25	0.0235
	$4\,^2A''$	3.43	0.0059
	$1\,^2A'$	4.32	0.0029
	$5\,^2A''$	4.41	0.1023

their f-values for excitation from D_0 all exceed the D_0−D_1 f-value, some by orders of magnitude. At least in principle, distortions along the 33 a' modes can mix D_1 with one or more of these states and impart intensity to the D_0−D_1 transition. To gain some heuristic sense of this possibility, approximate transition moment functions for selected a' modes were obtained from TD-B3LYP calculations at a series of normal coordinate displacements Q−Q_0 (Figure 10). Indeed, vibronic activity is implied to be rampant among a' modes, with one or both of the in-plane components of μ growing substantially away from Q_0, plainly accounting for the inutility of purely FC simulations.

5.3. Herzberg−Teller Analysis. To accommodate the dependence of μ on nuclear motion, the transition dipole moment connecting lower and upper vibronic states v'' and v' is expanded about Q_0 as a Taylor series in the normal coordinates $\{Q_i\}$ for each polarization direction, that is,

$$\boldsymbol{\mu}_{v'\leftarrow v''} = \boldsymbol{\mu}_0\langle v'|v''\rangle + \sum_{i=1}^{3N-6}\left(\frac{\partial \boldsymbol{\mu}}{\partial Q_i}\right)_0\langle v'|Q_i|v''\rangle + \frac{1}{2}\sum_{i,j=1}^{3N-6}\left(\frac{\partial^2 \boldsymbol{\mu}}{\partial Q_i \partial Q_j}\right)_0\langle v'|Q_iQ_j|v''\rangle + \ldots$$

The zeroth-order (*i.e.*, Condon) term represents the formally allowed $v' \leftarrow v''$ transition moment at Q_0; higher-order terms describe Herzberg−Teller activity (but many authors refer strictly to the linear term as the HT moment). The D_0−D_1 Condon term is small for MVB, but crucially, not zero, meaning that a' modes can induce additional vibronic intensity. If, in addition to being vibronically active, a totally symmetric mode is also FC-active because of a displacement along Q, none of the integrals in HT and higher terms are necessarily zero for transitions involving that mode. Further, for weakly allowed transitions, the Condon and higher moments may be similar in magnitude, making for nonintuitive intensity patterns in progressions and combination bands, and causing a breakdown of mirror symmetry between excitation and emission (*vide infra*). Only the first derivatives of the transition moment surface are computed in the available implementation of the FCHT procedure used for this work;[27] as such, rigorous agreement with experiment is not expected of calculated FCHT intensities. Nevertheless, they are instrumental in securing vibronic assignments.

5.3.1. cis-MVB. FCHT simulations comprise the middle traces of Figure 6 (*cis*-MVB DF) and Figure 11 (*cis*-MVB R2C2PI). The reference geometry Q_0 and normal coordinates $\{Q_i\}$ are those of the final state, *i.e.*, D_1 for excitation and D_0 for emission.[27] With the exception of ν_{30} (and to a lesser extent ν_{15}), the inclusion of HT moments admits a mostly qualitatively correct description of the D_0−D_1 transition. Beginning with the 0^0 DF spectrum, it is predicted that modes 32−28 dominate the region 200−1000 cm^{-1}; that 25_1^0 (the ring-breathe) should be one of the weaker a' fundamentals; and that 33_1^0 should be relatively insignificant. These predictions are borne out in the experimental DF spectrum, and with $2\nu_{48}$ (73 cm^{-1}) built onto each a' false origin as described in Section 5.2, essentially all of the observed features below 1800 cm^{-1} are accounted for.

Likewise, turning to the *cis*-MVB excitation spectrum, the FCHT simulation (again neglecting ν_{30}) compares respectably with observation (Figure 11). HT terms account for much of the transition moment for a' modes, as for the *cis* origin DF spectrum. The transitions 33_0^1 and 32_0^1 are enhanced by a factor of ∼5, and 31_0^1 and 25_0^1 increase 2-fold. For 33_0^1, 32_0^1, and 25_0^1, experimental intensities still exceed those of theory, but that could partly be a consequence that 412, 486, and 963 cm^{-1}, which are broader than the origin band, all comprise more than one transition.

From the assignments in Figure 11, we determine a scaling factor of 0.958 for the calculated *cis*-MVB D_1 frequencies

https://doi.org/10.1021/acs.jpca.1c04496
J. Phys. Chem. A 2021, 125, 6420−6436

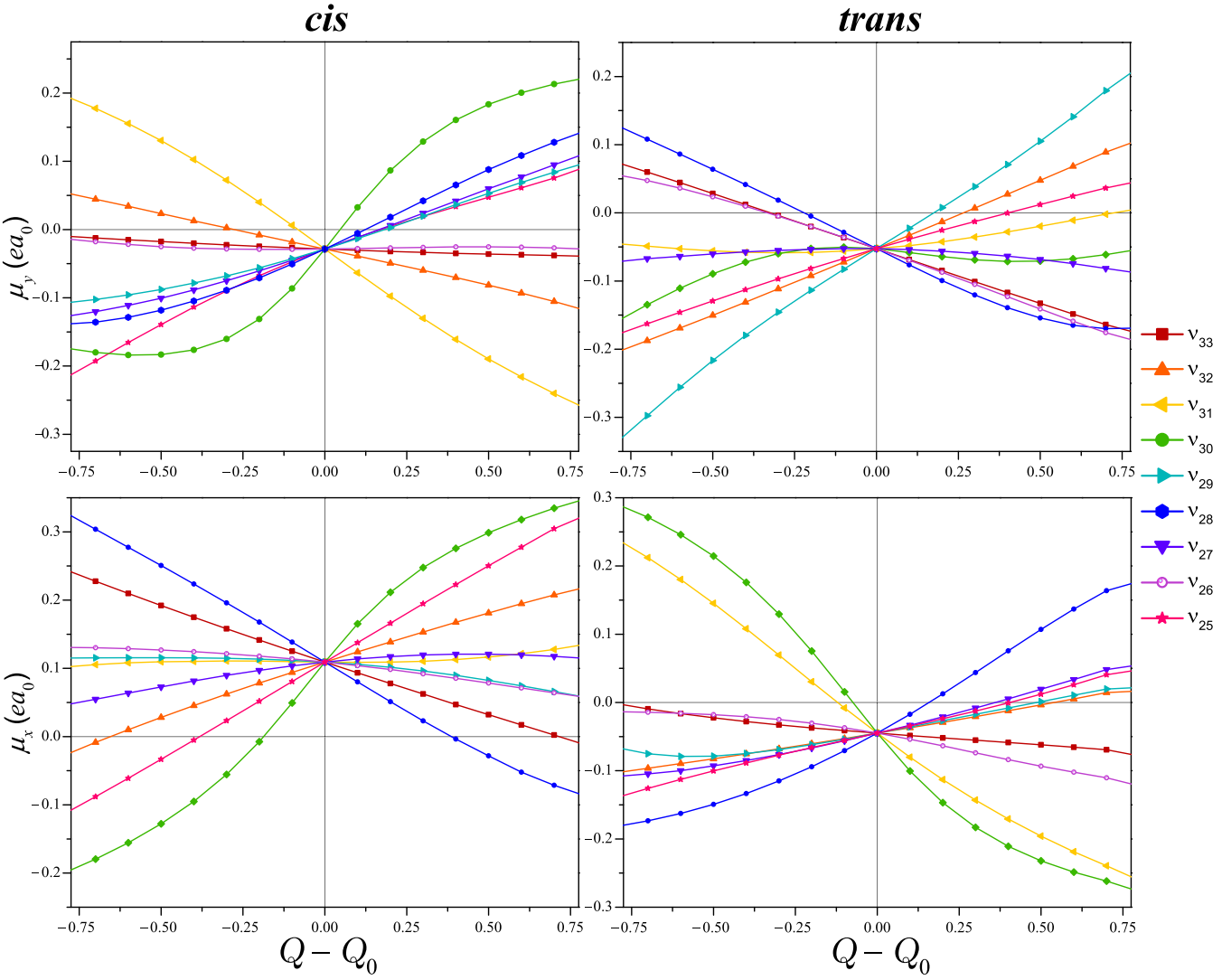

Figure 10. Calculated in-plane-polarized D_0−D_1 electronic transition moment functions μ_x and μ_y for selected a' modes of *cis*- (left) and *trans*-MVB (right). The transition moments are from TD-B3LYP calculations at a series of displacements along the D_0 normal coordinates Q_{33}−Q_{25}. The vertical axis of each plot spans 0.6 ea_0.

(Supporting Information, Section S6); this is consistent with results for similar systems,[20,21,31,32] giving us confidence in our analysis. Nevertheless, several assignments must be closely reasoned. The clearest discrepancy is that ν_{30} should be prominent in both emission and excitation spectra, but it exhibits middling strength in the former, and is apparently absent from the latter. While there is no plausible alternative assignment for the 525 cm^{-1} feature in DF, one might conjecture that the strong R2C2PI band at 282 cm^{-1}, which we assign as $46_0^1 48_0^1$, could instead be 30_0^1. This would require, however, that the calculated ν_{30} frequency is too high by *ca.* 18%.[60] It would furthermore imply the absence of $46_0^1 48_0^1$, unless the feature at 233 cm^{-1} has been misassigned; but then, the calculated ν_{46} frequency would be in error by *ca.* 40%. In contrast, our assignments for $46_0^1 48_0^1$ and $47_0^1 48_0^1$ yield D_1 ν_{46} and ν_{47} frequencies within *ca.* 4 and 7% of theory, respectively; further, they suggest 46_0^2 might appear near 380 cm^{-1}, where indeed at least one plausible candidate can be found nearby.

Moreover, transitions such as $46_0^1 48_0^1$, which engage the vinyl torsion and an out-of-plane bend, are commonplace in the S_0−S_1 spectra of styrene and its derivatives.[37,38,52−55] They are forbidden in the independent normal mode approximation but become allowed by Duschinsky rotation (as described in Section 5.1), often overshadowing the related FC-allowed overtones, and having intensities comparable to low-frequency totally symmetric fundamentals.[57] For styrene, where the lowest-frequency a'' modes undergo similar changes upon excitation to those of MVB, the total intensity carried by analogous transitions (involving modes 40−42) amounts to more than half of the origin intensity,[61] which is consistent with our assignments. That $46_0^1 48_0^1$ is stronger than predicted implies the mutual rotation of low-frequency modes has not been well described by theory,[62] which is hardly surprising given that ν_{48}'' is obviously highly anharmonic. In MVB, as in styrene, Duschinsky mixing involving the vinyl torsion is electronic in origin. The C1−C1′ bond attains significant double-bond character upon electronic excitation; the vinyl torsion frequency thus increases dramatically, becoming less disparate from other a'' modes, and causing strong mode-mixing.[51] Such coupling is much weaker in the ground state, as the vinyl torsion has a vastly lower frequency than any other a'' mode; the corresponding transition in emission ($46_1^0 48_1^0$, in our example) is thus weak (perhaps responsible for signal near 235 cm^{-1}), but the "pure" vinyl torsion overtone, 48_2^0, is prominent.

https://doi.org/10.1021/acs.jpca.1c04496
J. Phys. Chem. A 2021, 125, 6420−6436

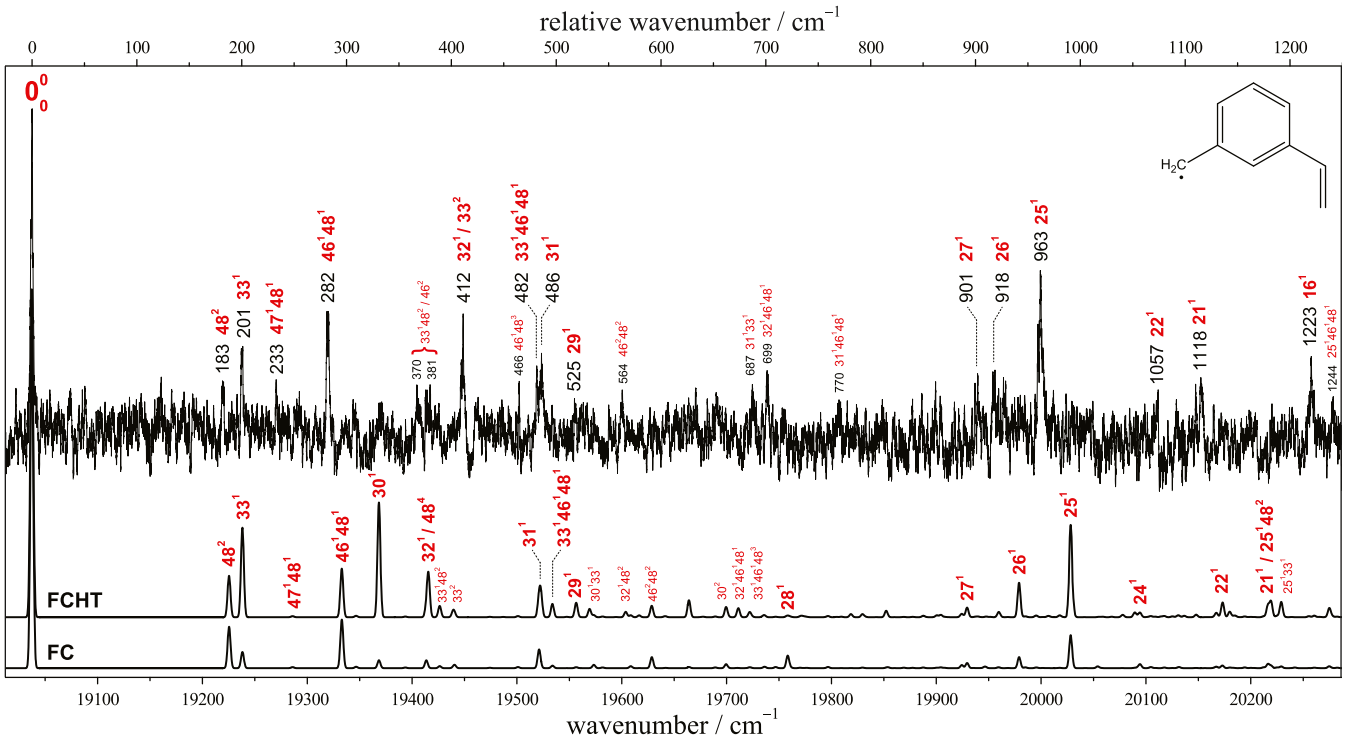

Figure 11. Optical−optical hole-burning spectrum obtained with the burn laser fixed to the *cis* origin transition, and beneath, simulations of the *cis*-*m*-vinylbenzyl electronic spectrum in the Franck−Condon Herzberg−Teller (FCHT) and Franck−Condon (FC) approximations, respectively. Each spectrum is intensity-normalized relative to its origin band.

This is also consistent with the S_0-S_1 origin DF spectrum of styrene, in which 42_2^0 and 42_4^0 have roughly 20 and 2.5% of the origin intensity, respectively, while the cross-sequence bands are relatively weak.[57]

We are thus confident in our assignment of $0^0 + 282$ cm^{-1} as $46_0^1 48_0^1$ and conclude that the calculated intensity of ν_{30} is erroneously high. It is perhaps no coincidence that the transition moment function for ν_{30} is highly nonlinear (Figure 10). To the extent that the above Taylor series expansion of $\boldsymbol{\mu}(Q)$ provides a useful description of vibronic intensities, the more stark disagreements between experiment and FCHT simulations owe in some measure to the neglect of higher-order terms. The calculation of such terms is relatively nontrivial, particularly if Duschinsky mixing is important; nevertheless, some inferences can be drawn from the signs of the diagonal contributions (*i.e.*, of the form $\left(\frac{\partial^n \boldsymbol{\mu}}{\partial Q^n}\right)\langle v'|Q^n|v''\rangle$). If the ath totally symmetric mode is HT-active and modestly displaced along the coordinate Q_a upon excitation, the integrals $\langle 1'_a|Q_a|0''\rangle$ and $\langle 1'_a|Q_a^3|0''\rangle$ are similar in magnitude and carry the same sign, and likewise for the analogous transition in emission. On the other hand, the *cis*-MVB ν_{30} transition moment function (Figure 10) is dominated by the Q_{30} and Q_{30}^3 terms, which have coefficients of similar magnitude but opposite sign. Thus, the linear and cubic diagonal moments for 30_0^1 and 30_1^0 interfere destructively. Without wanting to belabor this argument, it is possible that lesser discrepancies (*e.g.*, the FCHT relative intensities of 33_0^1 and 32_0^1 are roughly the inverse of the experiment) can be similarly explained, at least in part. For the S_1-S_0 spectrum of phenylacetylene, for example, it has been shown that all moments up to second order must be included to satisfactorily describe intensities in several a_1 modes.[63]

5.3.2. Asymmetry of Excitation and Emission Spectra. A striking feature of the *cis*-MVB excitation and emission spectra is an absence of mirror symmetry in the intensities of several a' modes. Most notably, the ν_{25} and ν_{33} fundamentals are conspicuous in excitation, but absent or weak in emission; and conversely, ν_{28} is the brightest a' mode in emission but is undetectable in excitation. The asymmetry is not due to Duschinsky rotation (as in fluorobenzene, for example[50]) because the three modes exhibit no significant off-diagonal matrix elements (Figure 9). It owes instead to interference between Franck−Condon and Herzberg−Teller (and possibly higher-order) moments, an effect first described by Craig and Small in connection with the 340 nm transition of phenanthrene.[64] Its origin is explained in Figure 12, adapted from ref 65. An electronic transition displaces the equilibrium geometry of the molecule along the normal coordinate Q of a totally symmetric mode. For the fundamental transitions of that mode, the integrands for the FC term are of opposite sign in excitation *vs* emission, but there is no change in the sign for the HT integrands. Thus, if the FC and HT moments reinforce for one process, they will cancel for the other. Because the intensity of a transition depends on the square of the transition moment, the asymmetry can be pronounced when the two moments have similar magnitudes. A comparison of the FC and FCHT simulations shows that for ν_{25} and ν_{33}, the FC and HT terms interfere constructively for excitation and destructively for emission, and *vice versa* for ν_{28}, which should be negligible in excitation. These predictions correspond well with experiment.

5.3.3. trans-MVB. Figure 13 shows the MVB R2C2PI spectrum with *trans* FC and FCHT simulations. Known features of *cis*-MVB are shown in reduced opacity.[66] In the FCHT simulation, intensities of all transitions appearing

https://doi.org/10.1021/acs.jpca.1c04496
J. Phys. Chem. A 2021, 125, 6420−6436

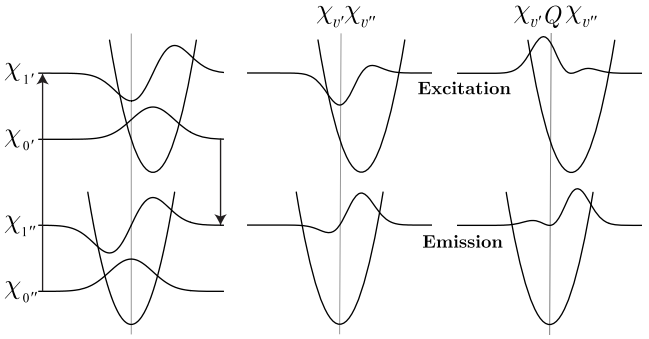

Figure 12. Illustration of sign behavior of integrands in FC (middle panel) and FCHT (right panel) terms for 1−0 excitation and 0−1 emission, assuming a positive displacement along the normal coordinate Q for the excited-state minimum, relative to ground. Reprinted (Adapted or Reprinted in part) with permission from Hohlneicher, G., and Wolf, J., *Ber. Bunsenges. Phys. Chem.* **1995**, 99(3), 366−370. Copyright 1995 Wiley-VCH.[65]

between 33_0^1 and 18_0^1 have been scaled (×2) to facilitate comparison with experiment. While many observed and calculated intensities still differ considerably, the FCHT simulation provides crucial qualitative guidance for securing assignments. Significant strength is implied in several a' modes—notably 33, 29, 28, and 18—that carry relatively modest FC intensity; and the ring-breathe (ν_{26}) is correctly predicted to be weak because of destructive FC-HT interference. It is clear why the *trans* spectrum, in contrast to the *cis* spectrum, is not origin-dominated, even though the two conformers should exhibit similar FC activity: the transition moment gradients for a' modes are of similar magnitude for both conformers (Figure 10), but *trans*-MVB has a roughly 3-fold smaller Condon moment. The origin (indeed, any transition) is enhanced (or diminished) by HT moments of all FCHT-active a' modes, but the size of the effect can be small relative to certain $\Delta v = 1$ transitions. By way of heuristic explanation, the HT terms for the origin $0' \leftarrow 0''$, and for one quantum of excitation $1'_a \leftarrow 0''$ in a totally symmetric mode, FCHT-active mode a can be written as

$$\boldsymbol{\mu}_{0'\leftarrow 0''}(\mathrm{HT}) = \langle 0'|0''\rangle \sum_i \frac{\partial \boldsymbol{\mu}}{\partial Q_i} \underbrace{\frac{\langle 0'_i|Q_i|0''_i\rangle}{\langle 0'_i|0''_i\rangle}}_{\ll 1}$$

$$\boldsymbol{\mu}_{1'_a\leftarrow 0''}(\mathrm{HT}) = \langle 0'|0''\rangle \left(\frac{\partial \boldsymbol{\mu}}{\partial Q_a} \frac{\langle 1'_a|Q_a|0''_a\rangle}{\langle 0'_a|0''_a\rangle} + \underbrace{\frac{\langle 1'_a|0''\rangle}{\ll 1}} \sum_{i\neq a} \frac{\partial \boldsymbol{\mu}}{\partial Q_i} \frac{\langle 0'_i|Q_i|0''_i\rangle}{\langle 0'_i|0''_i\rangle} \right)$$

where $\langle 0'|0''\rangle = \prod_{j=1}^{3N-6}\langle 0'_j|0''_j\rangle$ for independent normal modes in the absence of Duschinsky rotation, and the inequalities hold if normal coordinate displacements and changes in vibrational frequencies between the two electronic states are small, as is generally true of extended π-chromophores. The origin may thus be relieved of its dominance.

When scaled by 0.967, TD-B3LYP frequencies agree quite well with the experiment (Supporting Information, Section

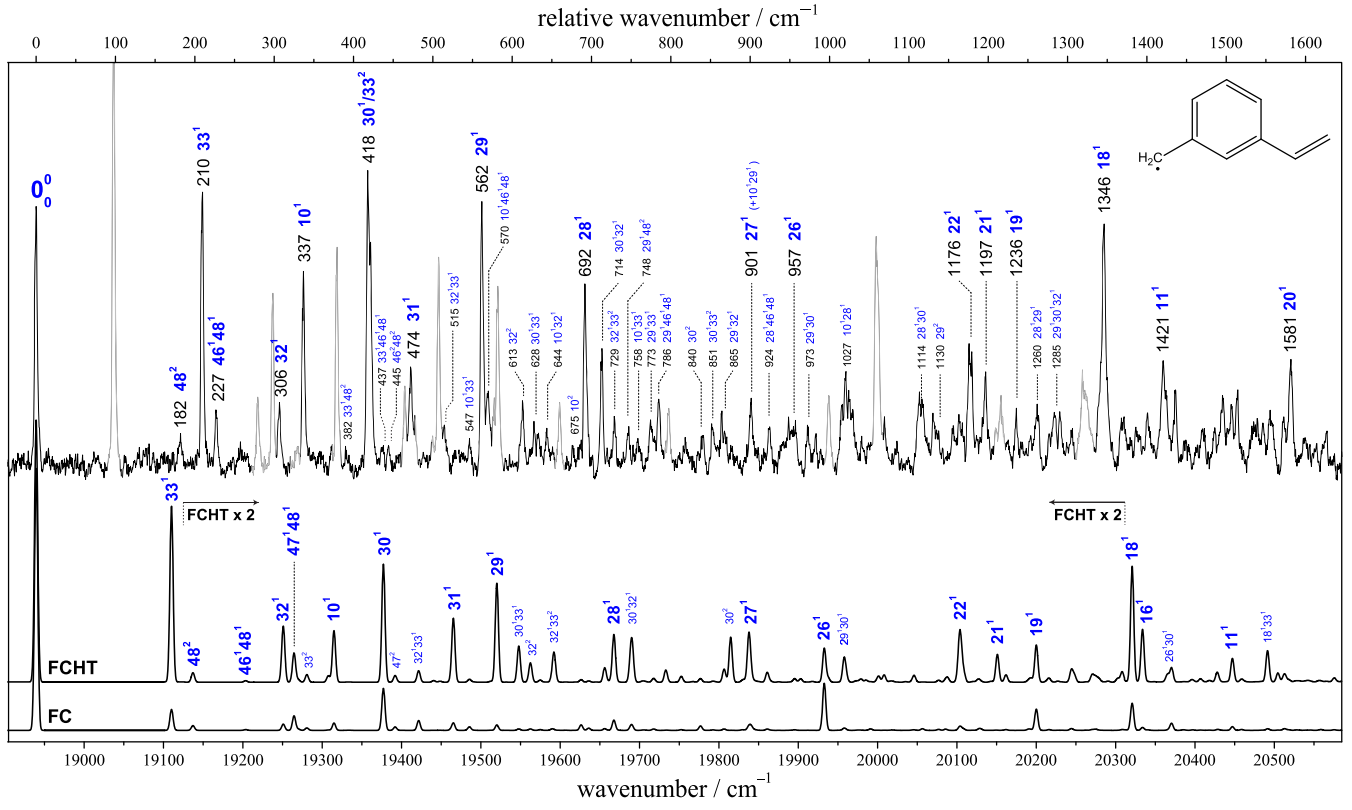

Figure 13. R2C2PI spectrum of *m*-vinylbenzyl, and beneath, simulations of the *trans-m*-vinylbenzyl electronic spectrum in the Franck−Condon Herzberg−Teller (FCHT) and Franck−Condon (FC) approximations, respectively. Light gray bands in the experimental spectrum are features of the *cis* isomer, identified by hole-burning spectroscopy. Each spectrum is intensity-normalized relative to its origin band. In the FCHT simulation, all transitions to levels between 33^1 and 18^1 have been scaled (×2) to facilitate comparison with the experiment.

https://doi.org/10.1021/acs.jpca.1c04496
J. Phys. Chem. A 2021, 125, 6420−6436

S6). Some frequencies derive from tentative assignments, particularly for weak bands in congested regions. Nevertheless, the scaling factor is again consistent with other RSRs[20,21,31,32] and is not dissimilar to that found for *cis*-MVB (0.958), which was determined from relatively few assignments. Still, a number of clearly discrepant FCHT intensities warrant further discussion. Some experimental bands may appear relatively strong simply because they comprise multiple transitions—for example, the relatively broad 1346 cm^{-1} band may contain both 18_0^1 and 16_0^1.

The justification for several other assignments is rather more nuanced—particularly for modes 10 and 32. The assignment of 33_0^1 was confirmed by DF, which leaves no reasonable alternatives for 48_0^2 and $46_0^148_0^1$. However, there are several possibilities for the bands at 306 and 337 cm^{-1}. The simulation implicates 32_0^1 and 10_0^1 as the strongest features nearby, while $47_0^148_0^1$, which might be expected close to 32_0^1, is predicted as the strongest of the vinyl torsion cross-sequence transitions. Again, we argue that the mutual rotation of modes 46−48 has been mischaracterized by theory. The observed $46_0^148_0^1$ intensity exceeds prediction by at least an order of magnitude. A Fermi-resonance with 33_0^1 is a possible cause, but the 33_0^1 DF spectrum (Supporting Information, Figure S3) shows no evidence of emission to 46_148_1. If $47_0^148_0^1$ were identified with either the 306 cm^{-1} or the 337 cm^{-1} band, the total intensity in the transitions 48_0^2, $46_0^148_0^1$, and $47_0^148_0^1$ would amount to either at least 50% or more than 100% of the origin intensity. It would thus follow that FC activity in the vinyl torsion and its Duschinsky-mixed cohorts for *trans* is similar to or stronger than that for *cis*. However, it is clear that electronic excitation affects a much greater change in the *cis* vinyl torsion potential than for *trans*, thereby engendering stronger FC activity: for example, the torsional overtone cannot be identified in the *trans* 0^0 DF spectrum (Supporting Information, Figure S3), but it dominates the *cis* DF spectrum at 73 cm^{-1} (Figure 6).

It thus seems more reasonable to assign the features at 306 and 337 cm^{-1} as 32_0^1 and 10_0^1, respectively. The D_1 "mode 10" is so labeled largely as a matter of convenience, according to the *trans* a' Duschinsky matrix in Figure 9. In terms of the D_0 basis, it mostly contains the character of modes 32 and 31, both evident in the *trans* 0^0 DF spectrum (Supporting Information, Figure S3). These modes derive most of their intensity from HT activity and can thus be observed in excitation and emission. In contrast we note, as for *cis*, pronounced intensity asymmetry for modes 33 and 28, for which the FC factors are relatively significant: both are bright in excitation, but weak or absent in emission.

Neglect of higher moments may, as for *cis*, account for some of the disagreement between observed and FCHT intensities. For phenylacetylene, the inclusion of second-order terms produces a nearly 2-fold enhancement in several a' modes.[63] The effect may be particularly substantial for overtones involving FCHT-active a' modes even if the higher derivatives of $\boldsymbol{\mu}(Q)$ are small, because the integrals $\langle n'_a|Q''_a|0''\rangle$, for an upper level with n quanta in the ath mode, will be significant for small displacements. For example, the strong, broad 418 cm^{-1} band, which clearly involves at least two levels, could derive much of its intensity from the diagonal second-order contribution to 33_0^2, expected near 420 cm^{-1}. The other component of the same band, assigned as 30_0^1, could gain intensity both from higher moments and from an anharmonic resonance with 33_0^2. Such resonances are probably common even at low energy owing to a mounting density of states of the same symmetry; more than one plausible zero-order assignment could have been suggested for almost every combination band above *ca.* 600 cm^{-1}. Our assignments for such combinations are based on the constituent frequencies, allowing for modest anharmonicities, but the intensities, which in addition to anharmonic coupling are sensitive to the mixed partial derivatives in $\boldsymbol{\mu}(Q)$, do not follow expected patterns, insofar as no intense transition serves as a false origin. Several of the proposed assignments should be testable by single vibronic level DF, which we defer until we can produce cold MVB radicals in higher abundance.

5.4. Astrochemical Relevance and Other Isomers. In a jet-cooled discharge of 1,6-heptadiyne, Steglich et al. recently detected C_9H_9 radicals in the region 630−550 nm by R2C2PI.[22] Several features were observed in close proximity to DIB wavelengths. The spectrum was tentatively ascribed to vinylbenzyl(s) from B3LYP/TD-B3LYP calculations and an AIE of 7.3 ± 0.1 eV measured for the carrier of an origin near 629 nm. It is now clear that MVB can be ruled out. Moreover, because their AIEs should be lower than that of MVB (7.17 eV), *o*- and *p*-vinylbenzyl can probably also be excluded. We have so far observed no optical absorption attributable to *o*- or *p*-vinylbenzyl in discharges of *o*- or *p*-vinyltoluene, under the same experimental conditions that yield MVB from *m*-vinyltoluene. It could be that the ortho isomer rearranges to 1-indanyl in the discharge, while the para isomer appears to decompose efficiently to *p*-ethynylbenzyl (C_9H_7), the identification of which we shall describe in detail elsewhere.

During recent work on the 1,6-heptadiyne discharge in our laboratory, we discovered 3-ethynylcyclopentenyl (*c*-C_5H_6−C≡CH) by R2C2PI near 459 nm. It is a highly resonance-stabilized isomer of C_7H_7 that contains a 1-vinylpropargyl chromophore. Its extension by vinyl substitution at the ethynyl terminus would yield an extensively delocalized C_9H_9 radical with a red-shifted spectrum, but the likely size of the red shift is not intuitively obvious. Empirically, it has been observed that the extension of a linear π-chromophore by ethynyl substitution red-shifts its absorption by *ca.* 60 nm.[16] However, vinyl substitution of allyl[67] and propargyl[30] causes a red shift of roughly 110 nm, implying vinyl-substituted 3-ethynylcyclopentenyl motifs deserve consideration in connection with the laboratory 630−550 nm bands. If the carriers fluoresce, DF spectroscopy should permit their diagnosis.

6. CONCLUSIONS

We have observed both conformers of *m*-vinylbenzyl under jet-cooled conditions by mass-resolved and fluorescence spectroscopies. Comparison of styrene/*m*-vinylbenzyl with the benzene/benzyl system gives a predicted D_0−D_1 transition energy in excellent agreement with the experiment. Dispersed fluorescence, hole-burning measurements, and torsional eigenstate calculations admit a conformer-specific assignment of the major features. B3LYP vibrational frequencies agree tolerably well with observed band positions when appropriately scaled, but a Franck−Condon description of relative band intensities is almost wholly inaccurate. The transition can only be qualitatively understood by considering pervasive Herzberg−Teller activity in totally symmetric modes and its interplay with Franck−Condon contributions to the transition moment. The FC and HT moments are of similar magnitude for several a' fundamentals but may have the same or opposite sign, causing some pronounced asymmetries between excitation and emission intensities. We have not yet optically

https://doi.org/10.1021/acs.jpca.1c04496
J. Phys. Chem. A 2021, 125, 6420−6436

detected the ortho and para isomers; the former may isomerize to 1-indanyl, while in the *p*-vinyltoluene discharge, which should yield the latter, we find *p*-ethynylbenzyl (C_9H_7). It would appear that no vinylbenzyl motif is responsible for C_9H_9 absorption bands observed in a 1,6-heptadiyne discharge throughout 630−550 nm, the carriers of which thus remain unidentified. Chromophores derived from vinyl substitution of 3-ethynylcyclopentenyl (C_7H_7), which is optically conspicuous in the heptadiyne discharge, may be plausible candidates.

■ ASSOCIATED CONTENT

Supporting Information

The Supporting Information is available free of charge at https://pubs.acs.org/doi/10.1021/acs.jpca.1c04496.

Trans-MVB hole-burning scan and DF spectra from levels 0^0 and 33^1 (0^0 + 210 cm^{-1}); D_0 and D_1 torsional potentials, eigenfunctions, eigenvalues, and discussion of Franck−Condon factors; simulated two-color ion-yield curves; optimized Cartesian coordinates and all calculated harmonic vibrational frequencies of D_0 and D_1 states of *cis*- and *trans*-MVB; and linear fits to observed *vs* calculated vibrational frequencies (PDF)

■ AUTHOR INFORMATION

Corresponding Author

Neil J. Reilly − *Department of Chemistry, University of Massachusetts Boston, Boston, Massachusetts 02125, United States;* orcid.org/0000-0001-5572-4784; Email: neil.reilly@umb.edu.

Authors

Sederra D. Ross − *Department of Chemistry, University of Massachusetts Boston, Boston, Massachusetts 02125, United States*

Jonathan Flores − *Department of Chemistry, University of Massachusetts Boston, Boston, Massachusetts 02125, United States*

Daniel M. Hewett − *Department of Chemistry, University of Massachusetts Boston, Boston, Massachusetts 02125, United States*

Complete contact information is available at: https://pubs.acs.org/10.1021/acs.jpca.1c04496

Notes

The authors declare no competing financial interest.

■ ACKNOWLEDGMENTS

This research was supported by awards from the US National Science Foundation (grant no. CHE: 1665341) and the American Chemical Society Petroleum Research Fund (Doctoral New Investigator Grant no. 57533-DNI6). S.D.R. acknowledges the US National Science Foundation for a Graduate Research Fellowship. J.F. thanks Oracle for the fellowship support during this project.

■ REFERENCES

(1) Buckingham, G. T.; Porterfield, J. P.; Kostko, O.; Troy, T. P.; Ahmed, M.; Robichaud, D. J.; Nimlos, M. R.; Daily, J. W.; Ellison, G. B. The Thermal Decomposition of the Benzyl Radical in a Heated Micro-reactor. II. Pyrolysis of the Tropyl Radical. *J. Chem. Phys.* **2016**, *145*, No. 014305.

(2) Buckingham, G. T.; Ormond, T. K.; Porterfield, J. P.; Hemberger, P.; Kostko, O.; Ahmed, M.; Robichaud, D. J.; Nimlos, M. R.; Daily, J. W.; Ellison, G. B. The Thermal Decomposition of the Benzyl Radical in a Heated Micro-reactor. I. Experimental Findings. *J. Chem. Phys.* **2015**, *142*, No. 044307.

(3) McEnally, C. S.; Pfefferle, L. D.; Atakan, B.; Kohse-Höinghaus, K. Studies of Aromatic Hydrocarbon Formation Mechanisms in Flames: Progress Towards Closing the Fuel Gap. *Prog. Energy Combust. Sci.* **2006**, *32*, 247−294.

(4) Miller, J. A.; Melius, C. F. Kinetic and Thermodynamic Issues in Formation of Aromatic Compounds in Flames of Aliphatic Fuels. *Combust. Flame* **1992**, *91*, 21−39.

(5) Miller, J. A.; Klippenstein, S. J. The Recombination of Propargyl Radicals and Other Reactions on a C_6H_6 Potential. *J. Phys. Chem. A* **2003**, *107*, 7783−7799.

(6) Richter, H.; Howard, J. B. Formation and Consumption of Single-Ring Aromatic Hydrocarbons and Their Precursors in Premixed Acetylene, Ethylene and Benzene Flames. *Phys. Chem. Chem. Phys.* **2002**, *4*, 2038−2055.

(7) Melius, C. F.; Colvin, M. E.; Marinov, N. M.; Pitz, W. J.; Senkan, S. M. In *Reaction Mechanisms in Aromatic Hydrocarbon Formation Involving the C5H5 Cyclopentadienyl Moiety*, Twenty-sixth Symposium (International) on Combustion, The Combustion Institute, Pittsburgh, 1996; pp 685−692.

(8) Long, A. E.; Merchant, S. S.; Vandeputte, A. G.; Carstensen, H.-H.; Vervust, A. J.; Marin, G. B.; Van Geem, K. M.; Green, W. H. Pressure Dependent Kinetic Analysis of Pathways to Naphthalene from Cyclopentadienyl Recombination. *Combust. Flame* **2018**, *187*, 247−256.

(9) Mebel, A. M.; Landera, A.; Kaiser, R. I. Formation Mechanisms of Naphthalene and Indene: From the Interstellar Medium to Combustion Flames. *J. Phys. Chem. A* **2017**, *121*, 901−926.

(10) Matsugi, A.; Miyoshi, A. Computational Study on the Recombination Reaction between Benzyl and Propargyl Radicals. *Int. J. Chem. Kinet.* **2012**, *44*, 206−218.

(11) Colket, M. B.; Seery, D. J. In *Reaction Mechanisms for Toluene Pyrolysis*, Twenty-fifth Symposium (International) on Combustion; The Combustion Institute, Pittsburgh, 1994; pp 883−891.

(12) Cherchneff, I.; Barker, J. R.; Tielens, A. G. G. M. Polycyclic Aromatic Hydrocarbon Formation in Carbon-rich Stellar Envelopes. *Astrophys. J.* **1992**, *401*, 269−287.

(13) Cherchneff, I. The Formation of Polycyclic Aromatic Hydrocarbons in Evolved Circumstellar Environments. *EAS Publications Series* **2011**, *46*, 177−189.

(14) Allamandola, L. J.; Tielens, A. G. G. M.; Barker, J. R. Polycyclic Aromatic Hydrocarbons and the Unidentified Infrared Emission Bands: Auto Exhaust along the Milky Way. *Astrophys. J.* **1985**, *290*, L25−L28.

(15) Johansson, K. O.; Head-Gordon, M. P.; Schrader, P. E.; Wilson, K. R.; Michelsen, H. A. Resonance-stabilized Hydrocarbon-Radical Chain Reactions May Explain Soot Inception and Growth. *Science* **2018**, *361*, 997−1000.

(16) Schmidt, T. The Electronic Spectroscopy of Resonance-Stabilised Hydrocarbon Radicals. *Int. Rev. Phys. Chem.* **2016**, *35*, 209−242.

(17) Polino, D.; P, M. Combustion Chemistry *via* Metadynamics: Benzyl Decomposition Revisited. *J. Phys. Chem. A* **2015**, *119*, 978−989.

(18) da Silva, G.; Cole, J. A.; Bozzelli, J. W. Thermal Decomposition of the Benzyl Radical to Fulvenallene (C_7H_6) + H. *J. Phys. Chem. A* **2009**, *113*, 6111−6120.

(19) Troy, T. P.; Nakajima, M.; Chalyavi, N.; Clady, R. G. C. R.; Nauta, K.; Kable, S. H.; Schmidt, T. W. Identification of the Jet-Cooled 1-Indanyl Radical by Electronic Spectroscopy. *J. Phys. Chem. A* **2009**, *113*, 10279−10283.

(20) Troy, T. P.; Chalyavi, N.; Menon, A. S.; O'Connor, G. D.; Fückel, B.; Nauta, K.; Radom, L.; Schmidt, T. W. The Spectroscopy and Thermochemistry of Phenylallyl Radical Chromophores. *Chem. Sci.* **2011**, *2*, 1755−1765.

(21) Sebree, J. A.; Kidwell, N. M.; Buchanan, E. G.; Zgierski, M. Z.; Zwier, T. S. Spectroscopy and Ionization Thresholds of π-

Isoelectronic 1-Phenylallyl and Benzylallenyl Resonance-Stabilized Radicals. *Chem. Sci.* **2011**, *2*, 1746−1754.
(22) Steglich, M.; Maity, S.; Maier, J. P. Visible Absorptions of Potential Diffuse ISM Hydrocarbons: C_9H_9 and C_9H_5 Radicals. *Astrophys. J.* **2016**, *830*, No. 145.
(23) Reilly, N. J.; Kokkin, D. L.; Ward, M. L.; Flores, J.; Ross, S. D.; McCaslin, L. M.; Stanton, J. F. Gas-Phase Optical Detection of 3-Ethynylcyclopentenyl: A Resonance-Stabilized C_7H_7 Radical with an Embedded 1-Vinylpropargyl Chromophore. *J. Am. Chem. Soc.* **2020**, *142*, 10400−10411.
(24) Campbell, E. K.; Maier, J. P. Perspective: C_{60}^+ and Laboratory Spectroscopy Related to Diffuse Interstellar Bands. *J. Chem. Phys.* **2017**, *146*, No. 160901.
(25) Thaddeus, P.; McCarthy, M. Carbon Chains and Rings in the Laboratory and in Space. *Spectrochim. Acta, Part A* **2001**, *57*, 757−774.
(26) Terentis, A. C.; Stone, M.; Kable, S. H. Dynamics of Acetaldehyde Dissociation at 308 nm: Rotational (N, K_a) and Translational Distributions of the HCO Photoproduct. *J. Phys. Chem. A* **1994**, *98*, 10802−10808.
(27) Barone, V.; Bloino, J.; Biczysko, M.; Santoro, F. Fully Integrated Approach to Compute Vibrationally Resolved Optical Spectra: From Small Molecules to Macrosystems. *J. Chem. Theory Comput.* **2009**, *5*, 540−554.
(28) Frisch, M. J. et al.*Gaussian 09*, Revision A.1; Gaussian Inc.: Wallingford CT, 2009.
(29) Reilly, N. J.; Nakajima, M.; Gibson, B. A.; Schmidt, T. W.; Kable, S. H. Laser-Induced Fluorescence and Dispersed Fluorescence Spectroscopy of Jet-Cooled 1-Phenylpropargyl Radical. *J. Chem. Phys.* **2009**, *130*, No. 144313.
(30) Reilly, N. J.; Nakajima, M.; Troy, T. P.; Chalyavi, N.; Duncan, K. A.; Nauta, K.; Kable, S. H.; Schmidt, T. W. Spectroscopic Identification of the Resonance-Stabilized cis- and trans-1-Vinylpropargyl Radicals. *J. Am. Chem. Soc.* **2009**, *131*, 13423−13429.
(31) Wilcox, C. M.; Krechkivska, O.; Nauta, K.; Schmidt, T. W.; Kable, S. H. Jet-Cooled Spectroscopy of ortho-Hydroxycyclohexadienyl Radicals. *J. Phys. Chem. A* **2018**, *122*, 8886−8897.
(32) Krechkivska, O.; Wilcox, C. M.; Nauta, K.; Kable, S. H.; Schmidt, T. W. Quantum-Induced Symmetry Breaking in the Deuterated Dihydroanthracenyl Radical. *J. Phys. Chem. A* **2019**, *123*, 6711−6719.
(33) Reilly, N. J.; da Silva, G.; Wilcox, C. M.; Ge, Z.; Kokkin, D. L.; Troy, T. P.; Nauta, K.; Kable, S. H.; McCarthy, M. C.; Schmidt, T. W. Interconversion of Methyltropyl and Xylyl Radicals: A Pathway Unavailable to the Benzyl-Tropyl Rearrangement. *J. Phys. Chem. A* **2018**, *122*, 1261−1269.
(34) Krechkivska, O.; Wilcox, C.; O'Connor, G. D.; Nauta, K.; Kable, S. H.; Schmidt, T. W. Ionization Energies of Three Resonance-Stabilized Radicals: Cyclohexadienyl (d_n, n = 0, 1, 6, 7), 1-Phenylpropargyl, and Methylcyclohexadienyl. *J. Phys. Chem. A* **2014**, *118*, 10252−10258.
(35) Pugliesi, I.; Müller-Dethlefs, K. The Use of Multidimensional Franck-Condon Simulations to Assess Model Chemistries: A Case Study on Phenol. *J. Phys. Chem. A* **2006**, *110*, 4657−4667. A free download of the software can be found at http://www.fclab2.net/index.html.
(36) Pugliesi, I.; Tonge, N. M.; Hornsby, K. E.; Cockett, M. C. R.; Watkins, M. J. An Examination of Structural Characteristics of Phenylacetylene by Vibronic and Rovibronic Simulations of Ab Initio Data. *Phys. Chem. Chem. Phys.* **2007**, *9*, 5436−5445.
(37) Hollas, J.; bin Hussein, M. Z. The 291-nm Band System of 3-Fluorostyrene: Gas-phase Absorption and Single Vibronic Level Fluorescence Spectra. *J. Mol. Spectrosc.* **1989**, *135*, 59−75.
(38) Hollas, J.; bin Hussein, M. Z. The 291-nm Band System of 3-Fluorostyrene: Ground State Vibrational Assignments for the *cis* and *trans* Rotamers from Their Supersonic Jet Spectra. *J. Mol. Spectrosc.* **1989**, *136*, 31−43.
(39) Dong, C.; Zhang, L.; Liu, S.; Hu, L.; Cheng, M.; Du, Y.; Zhu, Q.; Zhang, C. Rempi and Mati Spectroscopic Study of Selected *cis* and *trans*3-Chlorostyrene Rotamers. *J. Mol. Spectrosc.* **2013**, *292*, 35−46.
(40) Grassian, V. H.; Bernstein, E. R.; Secor, H. V.; Seeman, J. I. Conformational Study of Jet-Cooled Styrene Derivatives: Demonstration of the Planarity of Nonsterically Hindered Styrenes. *J. Phys. Chem. A* **1989**, *93*, 3470−3474.
(41) Western, C. M. *PGOPHER: A Program for Simulating Rotational, Vibrational and Electronic Spectra*, Journal of QuantitativeSpectroscopy and Radiative Transfer. http://dx.doi.org/10.1016/j.jqsrt.2016.04.010i, 2016.
(42) Pitzer, K. S.; Gwinn, W. D. Energy Levels and Thermodynamic Functions for Molecules with Internal Rotation I. Rigid Frame with Attached Tops. *J. Chem. Phys.* **1942**, *10*, 428−440.
(43) Spangler, L. H. Structural Information From Methyl Internal Rotation Spectroscopy. *Annu. Rev. Phys. Chem.* **1997**, *48*, 481−510.
(44) Wong, B. M.; Thom, R. L.; Field, R. W. Accurate Inertias for Large-Amplitude Motions: Improvements on Prevailing Approximations. *J. Phys. Chem. A* **2006**, *110*, 7406−7413.
(45) Lewis, J.; Malloy, T. B.; Chao, T. H.; Laane, J. Periodic Potential Functions for Pseudorotation and Internal Rotation. *J. Mol. Struct.* **1972**, *12*, 427−449.
(46) Longuet-Higgins, H. C.; Pople, J. A. The Electronic Spectra of Aromatic Molecules IV: Excited States of Odd Alternant Hydrocarbon Radicals and Ions. *Proc. Phys. Soc., Sect. A* **1955**, *68*, 591−600.
(47) O'Connor, G. D.; Woodhouse, G. V.; Troy, T. P.; Schmidt, T. W. Double-Resonance Spectroscopy of Radicals: Higher Electronic Excited States of 1- and 2-Naphthylmethyl, 1-Phenylpropargyl and 9-Anthracenylmethyl. *Mol. Phys.* **2015**, *113*, 2138−2147.
(48) Nam, S.; Cho, E.; Sim, E.; Burke, K. Explaining and Fixing DFT Failures for Torsional Barriers. *J. Phys. Chem. Lett.* **2021**, *12*, 2796−2804.
(49) Duschinsky, F. The Importance of the Electron Spectrum in Multi Atomic Molecules. Concerning the Franck-Condon Principle. *Acta Physicochim. URSS* **1937**, *7*, 551−566.
(50) Butler, P.; Moss, D. B.; Yin, H.; Schmidt, T. W.; Kable, S. H. Spectroscopy of the $\tilde{A}(^1B_2)-\tilde{X}(^1A_1)$ Transition of Jet-Cooled Fluorobenzene: Laser-Induced Fluorescence, Dispersed Fluorescence, and Pathological Fermi Resonances. *J. Chem. Phys.* **2007**, *127*, No. 094303.
(51) Smith, W. L. Intensities of Transitions in Non-Totally Symmetric Vibrations in the Electronic Spectra of Polyatomic Molecules. *J. Mol. Spectrosc.* **1996**, *176*, 95−98.
(52) Hollas, J. M.; Ridley, T. The $\tilde{A}^1A'$-$\tilde{X}^1A'$ Single Vibronic Level Fluorescence Spectrum of Styrene Vapor. *J. Mol. Spectrosc.* **1981**, *89*, 232−253.
(53) Smith, W. The Strong Duschinsky Effect and the Intensity of Transitions in Non-Totally Symmetric Vibrations in the Electronic Spectra of Polyatomic Molecules. *J. Mol. Spectrosc.* **1998**, *187*, 6−12.
(54) Hollas, J. M.; Taday, P. F. Methyl and Vinyl Torsional Potentials in cis- and trans-3-Methylstyrene from Supersonic Jet Fluorescence Spectra. *J. Chem. Soc., Faraday Trans.* **1991**, *87*, 3585−3593.
(55) Harper, C. M.; Hollas, J. The cis and trans Rotational Isomers of 3-Fluorostyrene. What Is the Energy Difference Between Them? *Chem. Phys. Lett.* **1994**, *226*, 577−582.
(56) Merrick, J. P.; Moran, D.; Radom, L. An Evaluation of Harmonic Vibrational Frequency Scale Factors. *J. Phys. Chem. A* **2007**, *111*, 11683−11700.
(57) Syage, J.; Adel, F. A.; Zewail, A. Jet-Cooled Styrene: Spectra and Isomerization. *Chem. Phys. Lett.* **1983**, *103*, 15−22.
(58) Knight, A. E. W.; Parmenter, C. S.; Schuyler, M. W. Extended View of the Benzene 260-nm Transition via Single Vibronic Level Fluorescence. I. General Aspects of Benzene Single Vibronic Level Fluorescence. *J. Am. Chem. Soc.* **1975**, *97*, 1993−2005.
(59) Knight, A. E. W.; Kable, S. H. The S_0-S_1 ($^1B_{2u}$-^1A_g) Transition of *p*-Difluorobenzene Cooled in a Supersonic Free Jet Expansion. Excitation and Dispersed Fluorescence Spectra, Vibrational Assignments, Fermi Resonances, and Forbidden Transitions. *J. Chem. Phys.* **1988**, *89*, 7139−7160.

https://doi.org/10.1021/acs.jpca.1c04496
J. Phys. Chem. A 2021, 125, 6420−6436

(60) A similar margin of error applies to 33_0^1 in the *trans* R2C2PI spectrum, but that mode has a relatively low frequency, it is clearly strongly vibronically active, and it may be perturbed by a Fermi-resonance with 48_0^2.
(61) Mahmoud, H.; Germanenko, I. N.; Ibrahim, Y.; El-Shall, M. S. Resonant Two-Photon Ionization Spectroscopy of Styrene (Methanol)$_n$ Clusters, n = 1 − 9. *J. Phys. Chem. A* **2003**, *107*, 5920−5932.
(62) The strength of the "forbidden" component depends on the rotation angle (specifically, the product cos θ sin θ, for two mutually rotated modes), in principle reaching a maximum at $\theta = 45°$[S1]
(63) Chang, C.-H.; Lopez, G.; Sears, T. J.; Johnson, P. M. Vibronic Analysis of the $S_1 - S_0$ Transition of Phenylacetylene Using Photoelectron Imaging and Spectral Intensities Derived from Electronic Structure Calculations. *J. Phys. Chem. A* **2010**, *114*, 8262−8270.
(64) Craig, D. P.; Small, G. J. Totally Symmetric Vibronic Perturbations and the Phenanthrene 3400Å Spectrum. *J. Chem. Phys.* **1969**, *50*, 3827−3834.
(65) Hohlneicher, G.; Wolf, J. Interference between Franck-Condon and Herzberg-Teller Contributions in Naphthalene and Phenanthrene. *Ber. BunsenGes. Phys. Chem.* **1995**, *99*, 366−369.
(66) Presumably many other weak features arise from the *cis* conformer, but are too weak to observe by holeburning given the present SNR.
(67) Chalyavi, N.; Bacskay, G. B.; Menon, A. S.; Troy, T. P.; Davis, N. J. L. K.; Radom, L.; Reid, S. A.; Schmidt, T. W. Spectroscopy and Thermochemistry of a Jet-Cooled Open-Shell Polyene: 1,4-Pentadienyl Radical. *J. Chem. Phys.* **2011**, *135*, No. 124306.

https://doi.org/10.1021/acs.jpca.1c04496
J. Phys. Chem. A 2021, 125, 6420−6436